Metabolic imprint of an intracellular pathogen drives histone hypermethylation and tunes the host transcriptional response to infection

Chloé I. Charendoff [1,2], Félix V. Louchez[1,2], Yongzheng Wu[1], Lee Dolat[3], Guillaume Velasco[4], Stéphanie Perrinet[1], Adrian Gabriel Torres[5, 6], Laure Blanchet[1,2], Magalie Duchateau[8], Quentin Giai Gianetto[8,9], Mariette Matondo[8], Laurence Del Maestro[4], Slimane Ait-Si-Ali[4], Frédéric Bonhomme[10], Gaël A. Millot[9], Lluís Ribas de Pouplana[5, 6, 7], Elisabeth D. Martinez[11], Raphael H. Valdivia[3] and Agathe Subtil[1#]

[1] Institut Pasteur, Université Paris Cité, UMR3691 CNRS, Cellular biology of microbial infecion, F-75015, Paris, France.

[2] Sorbonne Université, Collège Doctoral, F-75005 Paris, France

[3] Department of Integrative Immunobiology, Duke University School of Medicine, Durham, NC 27701

[4] UMR7216 Épigénétique et Destin Cellulaire, CNRS, Université Paris Cité, Epigenetics and Cell Fate, F-75013, Paris, France

[5] Institut de Recerca Biomèdica (IRB Barcelona), Barcelona, 08028, Catalonia, Spain.

[6] Barcelona Institute of Science and Technology (BIST), Barcelona, 08028, Catalonia, Spain.

[7] Institució Catalana de Recerca i Estudis Avançats (ICREA), Barcelona, 08010,Catalonia, Spain.

[8] Institut Pasteur, Université Paris Cité, CNRS UAR 2024, Proteomics Platform, Mass Spectrometry for Biology, Paris, France

[9] Institut Pasteur, Université Paris Cité, Bioinformatics and Biostatistics HUB, Paris, France

[10] Institut Pasteur, Université Paris Cité, UMR 3523 CNRS, Epigenetic Chemical Biology, F-75015 Paris, France

[11] Department of Pharmacology, UT Southwestern Medical Center, Dallas, TX, USA

Corresponding author. Email: asubtil@pasteur.fr Phone : +33 14061 3049

Keywords: *Chlamydia trachomatis*, intracellular pathogen, epigenetic, histone demethylase, innate immunity

ABSTRACT

Chlamydia trachomatis, an intracellular bacterium, highjacks metabolites from the host cell. We provide evidence of global hypermethylation of the host proteome, including histones, during the late stages of infection and that histone hypermethylation is the result of metabolic imbalance favoring the activity of lysine methyl transferases over demethylases. We find that histones hypermethylated at residues H3K4 and H3K9 are distributed throughout the chromatin. Inhibition of bacterial growth, or supplementation of the culture medium with iron or with dimethyl-ketoglutarate (DMKG) reduced histone hypermethylation. DMKG supplementation modified the transcription of about one third of the infection-responsive genes, including genes involved in the innate response to infection. Transfer RNA (tRNA) levels decreased late in infection and DMKG supplementation prevented this phenomenon. Finally, we uncovered a robust, histone demethylase dependent shut-down of the innate response in the mouse genital tract shortly after the acute phase of infection. Overall, our data show that the metabolic pressure exerted by a pathogen with an intracellular lifestyle drives an epigenetic imprint that tunes the transcriptional response of its host.

INTRODUCTION

Chemical modifications of histones or DNA determine chromatin condensation, DNA accessibility and recruitment of the transcription machinery. Methylation of DNA and histones are the best characterized chromatin modifications. In general, DNA methylation is associated with chromatin compaction and inhibition of transcription, while histone methylation can either promote or repress transcription depending on the specific histone and lysine residues modified (1).

Chromatin dynamics is regulated by cellular metabolism as several metabolites support chromatin remodeling. All methylation reactions rely on the availability of S-adenosyl methionine (SAM) (2) and numerous chromatin modifiers use metabolites as cofactors (3). The enzymatic activity of many histone lysine demethylases requires the 2-oxoglutarate oxygenase activity of its Jumonji C (JmjC) domain with 2-oxoglutarate (also known as α-ketoglutarate; aKG) and iron II (Fe(II)) needed for the demethylation reaction (4). The activities of the histone demethylases are sensitive to physiological variations in the concentration of these metabolites (or of competitive metabolites), and thereby metabolic changes can influence epigenetic modifications (5-7). Overall, the effect of metabolites on the epigenetic status of chromatin are well documented in metabolic diseases and in cancer (3, 8). Metabolites are also at the heart of the influence of the mammalian gut microbiota on host developmental, immunologic, and metabolic outcomes (9-12).

The obligate intracellular bacterium *Chlamydia trachomatis* infects epithelial cells of the genital tract and of the eye conjunctiva (13). The bacteria undergo a biphasic developmental cycle, which takes place entirely within a vacuolar compartment, called an inclusion, and lasts about 48 h *in vitro* (14). All metabolites required for bacterial growth are captured from the host cytoplasm. A decade ago, a seminal study revealed that several histone methylation marks were increased in epithelial cells infected with *C. trachomatis* (15) but the mechanism underlying this shift in chromatin dynamics during infection is unknown. Furthermore, marks normally associated with opposite outcomes in terms of gene expression, such as H3K4me3 and H3K9me3, were similarly upregulated at the population level, so that the global outcome of these changes on host transcription was not predictable.

Here, we characterized the nature of histone modification during *C. trachomatis* infection at the single cell level. We observed that the level of histone methylation was variable between infected cells, and that the proportion of cells that displayed a high level of histone methylation increased with infection time. Strikingly, at the individual cell level, the levels of methylation of different lysine residues strongly correlated with each other. At the proteome level we see an overall increase in protein methylation in infected cells. We provide evidence that hypermethylation on histone lysine residues is due to metabolic imbalance occurring late in infection that impairs the activity of demethylases. We mapped the deposition of two major marks, H3K4me3 and H3K9me3 and determined that the global remodeling of host chromatin affects the expression of genes implicated in the innate response of epithelial cells to infection. Finally, we provide evidence that the shut-down of the acute innate response to *Chlamydia* infection in the mouse genital tract requires histone demethylase activities.

RESULTS

C. trachomatis infection induces protein hypermethylation during late infection.

Several histone methylation marks (H3K4me3, H3K9me3, H3K27me3, H3K79me2, H4K20me3) were examined by immunofluorescence in cells infected for 48 h with *C. trachomatis* (serovar LGV-L2). All marks displayed a strong signal in several, but not all, infected cells (Fig. 1A). Strikingly, most cells positive for one mark were also positive for a second mark. An automated procedure to quantify fluorescence intensities in nuclei confirmed the increase in methylated histone lysine residues in nuclei of infected samples compared to non-infected ones (Fig. 1B), and the positive correlation between the intensities for the co-stained histone methylation marks (Fig. 1C). Histone lysine hypermethylation was not restricted to *C. trachomatis*, as the mouse adapted strain *C. muridarum* also induced histone hypermethylation late in infection in HeLa cells and in mouse embryonic fibroblasts (MEFs) (Fig. S1A-B). Histone hypermethylation in MEFs was also observed upon infection with *C. trachomatis* (Fig. S1B).

To validate these observations in non-cancer derived cells we first used primary epithelial cells derived from the ectocervix of female patients (16). The number of nuclei positive for the three histone methylation marks tested (H3K9me3, H3K27me3, H4K20me3) was significantly higher in the infected cells compared to non-infected cells (Fig.S1C). Finally, we used a mouse endometrial organoid model that recapitulates epithelial cell diversity, polarity and ensuing responses to *Chlamydia* infection (17). We observed an increase in H3K9me3 intensity in nuclei of infected cells, compared to the surrounding non-infected cells, when organoids were infected with *C. trachomatis* or *C. muridarum* (Fig. 1D). These observations confirm the ubiquity of global histone hypermethylation in the late stages of infection.

To understand whether histone post-translational modifications (PTMs) late in infection was specific to histones or the result of a general increase in protein methylation, we applied mass spectrometry-based bottom-up proteomics to assess the level of methylation of proteins in infected versus uninfected cells. Statistical analyses were performed on confidently identified methylated peptides encompassing mono-, di-, or tri-methylations. The changes in quantified values were compared to the changes of their belonging proteins quantified from non-modified peptides, to control for changes in protein relative abundance because of infection. These analyses revealed an increase in protein methylation in infection on arginine and lysine residues (Fig. 1E and Table S1). Despite the inherent challenges associated with the combinatorial nature of post-translational modifications on histones, we discerned hypermethylation of H3K79 in infected samples. Additional

methylated proteins included those implicated in mRNA synthesis (e.g. SUPT5H, TFIP11, HNRNPAB, HNRNPA2B1) and the cytoskeleton (tubulin alpha (TUBA3D) and keratin 18). In contrast, peptides associated to only one protein (HNRNPU) were found to be significantly less methylated in infected samples compared to non-infected ones. Finally, to assess whether hypermethylation extended to host DNA, we quantified the methylation level of cytosine residues in nuclei from infected vs. non-infected cells by LC-MS/MS analysis. In contrast to what we had observed on histones, host DNA was slightly hypomethylated in infected cells (Fig S1D). Altogether, we concluded that the hypermethylation of histones during *C. trachomatis* infection occurred in the context of global protein, not DNA, hypermethylation. Importantly, we did not observe significant changes in the abudance of known methyl transferases nor of demethylases in the proteomic data that could account for the hypermethylation profile (Table S2).

Histone hypermethylation is linked to bacterial metabolic activity but not to the bacterial effector Nue.

Histone hypermethylation was first detected 24 hours post infection (hpi) with the proportion of positive nuclei in the infected population increasing with time (Fig. 2.A). The addition of increasing doses of the antibiotic doxycycline to the culture medium for the last 24 h of the infection induced a dose-dependent reduction in the number of infectious bacteria collected 48 hpi (Fig. 2.B), and in the percentage of cells positive for H3K4me3 or H4K20me3 (Fig. 2.C). This result indicated that bacterial growth correlated with the levels of histone methylation. To confirm this finding, we developed an automated pipeline to discriminate nuclei of non-infected cells from nuclei of cells infected with *C. trachomatis* L2 expressing the fluorescent protein mCherry. We observed that, within the infected cells, the mean intensity of the mCherry signal was higher in cells that displayed hypermethylation of H3K9me3 than in cells with low level of H3K9me3, meaning that histone hypermethylation correlated positively with bacterial burden (Fig. 2D).

We next asked whether Nue, a protein secreted by *Chlamydia* endowed with histone methyl transferase activity (18), was implicated in this process. We obtained a *C. trachomatis* strain with a non-sense mutation in *nue* (C to T mutation at position 129786 leading to a W71* truncation), designated as CTL2M340 (19) and confirmed the absence of Nue expression by western blot analysis (Fig. S1E). Histone hypermethylation was still observed in cells infected for 48 h with CTL2M340, demonstrating that Nue is not required for histone hypermethylation observed late in infection (Fig. S1E).

Histone demethylation is deficient in late infected cells.

The histone methylation marks we found in infected cells are deposited by several types of histone methyl transferases and removed by an equally diverse set of dedicated demethylases (4, 20, 21). Because some of these enzymes use common co-factors we reasoned that availability of these co-factors during infection could account for the observation that several histone marks were affected simultaneously. Hypermethylation could be the result of increased methylation or decreased demethylase activity. Since all methylation reactions use SAM as a co-factor, we determined SAM concentrations from isolated host nuclei using a fluorescence transfer-based assay. We observed a 50% decrease in the amount of nuclear SAM in cells infected by *C. trachomatis* for 48 h, suggesting that histone hypermethylation is not a consequence of SAM accumulation during infection (Fig. 3A). We thus considered the possibility of a decrease in histone demethylase activity late in infection. To test this hypothesis, we first looked at whether a demethylase inhibitor could reproduce the histone hypermethylation phenotype. JIB-04 is a membrane permeable small inhibitor of all JmjC

demethylases (22). When applied at 2 μM in the culture medium for 24 h we observed a moderate increase in H4K20me3 signal in HeLa cells (Fig. 3B,C). When the inhibitor was applied 24 h after infection by *C. trachomatis*, and the cells fixed and stained 48 hpi, we observed a dose dependent increase in the H4K20me3 positive cells among the infected cells. A similar result was obtained for H3K9me3 (Fig S2A.B). The increase in histone methylation induced by JIB-04 treatment was much more pronounced in the infected than in the non-infected cells. Note that hypermethylation occurred despite a negative effect of JIB-04 treatment on bacterial development (Fig. S2C). These data indicate that infected cells are sensitized to the action of an inhibitor of JmjC demethylases, consistent with the hypothesis that lysine demethylation by JmjC demethylases is sub-optimal late in infection.

JmjC demethylases require oxygen, iron (FeII) and aKG, and any limitation in one of these three co-factors could impair their activity. Oxygen can be excluded, as the experiments are performed under normoxic conditions. If iron and/or aKG became limited during infection, supplementation of the culture medium with these metabolites should prevent histone hypermethylation, provided they are transported to the host cytoplasm. Iron was supplemented with addition of 100 μM ferric ammonium citrate in the culture medium, a concentration sufficient to reverse iron deficiency *in vitro* (7). For aKG we supplemented the culture medium with 5 mM dimethyl-ketoglutarate (DMKG), which is membrane permeable and converted into aKG by cytosolic esterases. Interestingly, we observed that changing the medium at mid-course during infection (24 hpi) was sufficient to partially reduce H3K4 and H4K20 tri-methylation at 48 hpi (Fig. 3D-E, DMSO alone). Supplementation of iron or DMKG reduced the level of histone methylation even further. To control for the possible effect of these treatments on bacterial growth, we measured their impact on the infectious forming units (IFUs) produced within 48 h. Iron supplementation had no effect on IFUs while DMKG supplementation reduced the infectious progeny by about 25% and combining iron and DMKG reduced progeny by about 50% (Fig. S2D). The effect of the combination was not tested as the reduction on bacterial growth could be sufficient on its own to prevent histone methylation. Altogether, these experiments show that DMKG or iron supplementation of the culture medium partially reverse hypermethylation of histone lysine residues late in infection. They strongly argue for the hypothesis that infection-driven depletion of their cytoplasmic concentrations leads to sub-optimal activity of JmjC histone demethylases.

If this hypothesis is correct, overexpression of a given JmjC demethylase should also reverse at least partially the phenotype on the specific residues it targets. We overexpressed KDM4A (also known as JMJD2A), specific for H3K9me3 and H3K36me3 with no activity on other methylation marks such as H3K4me3 (23). Cells were infected with mCherry expressing *C. trachomatis* L2 and transfected 2 hours later with HA-tagged KDM4A. To control for the potential effect of transfection on bacterial development control cells were transfected with an irrelevant construct expressing a truncated HA-tagged protein, HA-Tsg5' (24). We observed a 40% reduction in the proportion of infected cells that displayed H3K9me3 hypermethylation in cells expressing HA-KDM4A. In contrast, the proportion of infected cells positive for H3K4me3 was unchanged (Fig. 3FG). Thus, overexpression of KDM4A was sufficient to partially prevent hypermethylation of its specific target, H3K9. This result is fully consistent with the hypothesis that hypermethylation results from sub-optimal activity of histone demethylases, that can be specifically overcome by overexpression of a cognate demethylase.

Hypermethylation on H3K4 and H3K9 spreads throughout chromatin.

We investigated the pattern of chromosomal deposition of two well-studied histone methylation marks, H3K4me3 and H3K9me3, associated with active and repressed chromatin, respectively, in infected cells by chromatin immunoprecipitation followed by DNA sequencing (ChIP-seq). We

observed an increase in the amount of material immunoprecipitated from infected samples compared to non-infected samples, consistent with the increase of these methylation marks during infection (Fig S3A). Samples were adjusted to equal DNA concentration before sequencing. Peak calling showed that the number of peaks for H3K4me3 or H3K9me3 were not significantly changed (Fig. S3B). H3K4me3 mark was enriched in active promoters whereas H3K9me3 was enriched in heterochromatin and regions of low activity, as expected (Fig. S3C). Since the two independent experiments showed the expected hierarchical clustering (Fig. S3D) we merged the reads from biological replicates pairs for H3K4me3 and H3K9me3 for further analysis. The density of reads in H3K4me3 peaks diminished in infected samples (Fig 4A) and was accompanied by a slight but significant increase of the median of read coverage all over the genome in the immunoprecipitated fractions and not in the input (Fig. 4B). These data are consistent with H3K4 hypermethylation in infected cells occurring outside H3K4me3-enriched chromatin rather than reinforcing existing peaks. In other words, the inhibition of H3K4me3 demethylation increases the proportion of methylated H3K4 outside H3K4me3-enriched areas of chromatin. The median of read coverage all over the genome also increased slightly in the H3K9me3 immunoprecipitated fractions (Fig. 4B). The distribution of H3K9me3 over the different regions of chromatin was very conserved between infected and non-infected samples (Fig. S4C) and only 20 sites were significantly differentially enriched for H3K9me3 between the two conditions (Table S3). These data suggest that, while globally increasing late in infection, the pattern of deposition of H3K9me3 remained similar to that of non-infected cells.

DMKG supplementation modifies the host cell's transcriptional response to infection.

To assess the impact of histone methylation on the host's transcriptional responses, cells were infected with or without supplementing the culture medium with DMKG 24 hpi. Non-infected cells were treated in parallel. RNA was extracted from these cells 48 hpi and processed for analysis by microarray. The differentially expressed genes (DEGs) were defined with a cut-off of |Fold-increase|>2 and a p-value <0.05. The number of elements differentially up or down regulated between any conditions are split evenly (Fig. 5A). In non-treated samples, we observed 1055 genes were differentially regulated by infection (Fig. 5A and Table S4). About one third of those were no longer differentially expressed when DMKG was added to the culture medium, indicating that increasing intracellular levels of aKG during infection impacts on the host cell's transcriptional response to infection (Fig 5B).

To analyze this phenomenon further, we looked at the effect of DMKG supplementation on each condition. In non-infected cells, DMKG supplementation resulted in differential expression of 267 genes, evenly distributed between transcripts that were upregulated (133) and downregulated (134). In infected cells, a similar range of changes was observed, with 314 DEGs, 184 being up and 130 being down (Fig. 5A, Table S5). Among the 184 genes that were upregulated with DMKG supplementation in infection, 32 corresponded to transcripts that were upregulated by infection, and 62 to transcripts that were downregulated by infection (the remaining 90 elements showing less than a 2-fold difference in transcription upon infection). Therefore, the shift in transcription from infection to infection with DMKG supplementation does not have a global trend. In other words, DMKG supplementation enhances the transcription of some of the genes that were already upregulated by infection, while it dampens the transcription of others. The same observations were made on genes downregulated by infection. Thus, overall, the effect of DMKG supplementation on the expression of a given transcript depends on the transcript.

A discrete set of infection-responsive genes are highly sensitive to DMKG supplementation.

We had observed 267 DEGs in non-infected samples supplemented with DMKG compared to non-treated samples (Fig. 5A). To minimize the intrinsic effect of DMKG, we excluded from the 314 DEG list (comparison of infected and infected with DMKG supplementation) those that showed over 2-fold differential expression upon DMKG treatment alone, reducing the list to 246 DEGs. Among those, 91 correspond to genes that are differentially regulated by infection (Table S5). To validate the microarray data, we first tested by reverse transcription quantitative PCR (RT-qPCR) the mRNA levels of 5 genes displaying a strong response to infection (>2.5 fold difference between infected and non-infected samples) and a strong response to DMKG in infected samples (>2.5 fold difference between DMKG-treated and not-treated in infected samples). These genes code for the chemokine CCL20, the growth factor epigen (EPGN), the down regulator of MAPK Dual specificity protein phosphatase 6 (DUSP6), the methyltransferase-like protein 7A (METTL7A) and the interleukin-1 receptor like 1 (IL1RL1, also known as ST2). Alternative splicing of IL1RL1 generates a soluble form called sST2, which acts as a decoy receptor for interleukin 33 (IL-33) (25). We determined using specific primers that sST2 was the only isoform expressed during *C. trachomatis* infection, we thus refer to this gene as *sST2*. RNA was extracted at 48 hpi from infected vs non infected cells with and without DMKG supplementation at 24 hpi and compared to uninfected controls via RT-qPCR. The RT-qPCR results recapitulated the microarray data for the 5 genes tested, validating the quality of the microarray dataset (Fig. 5C). Since DMKG prevents histone lysine hypermethylation during infection, and JIB-04 has the reverse effect, we expected these genes to respond to DMKG and JIB-04 treatment in opposite ways. RNA was extracted at 48 hpi from infected vs. uninfected cells with and without treatment with 1 μM JIB-04 at 24 hpi and compared to uninfected controls. We observed a significant effect of JIB-04 on transcript levels of each of the 5 genes except DUSP6 (Fig. 5C). DMKG and JIB-04 had opposite effect on transcription of *sST2*, *CCL20* and *EPGN* (Fig. 5C). *CCL20*, which was upregulated by infection, was downregulated by DMKG supplementation and upregulated by JIB-04. *sST2* and *EPGN*, which were upregulated by infection and further upregulated by DMKG supplementation, were downregulated by JIB-04 supplementation. In contrast, DMKG and JIB-04 supplementation had the similar effect on *MTTL7A* transcripts level, *i.e.* they both exacerbated the infection-induced downregulation of this transcript. Thus, the level of expression of *METTL7A* does not appear to be ultimately governed by the histone lysine methylation status. Overall, we concluded from the analysis of the microarray dataset that a discrete number of genes that respond to infection are differentially regulated upon DMKG supplementation, and that, for several of those, the modulation of histone methylation levels could account for this effect.

The levels of host tRNAs decrease late in infection, an effect reversed by DMKG supplementation.

Only 116 of the 314 DMKG sensitive DEGs corresponded to protein coding transcripts (Table S5). The rest of the elements were non-coding RNAs like pseudogenes, lnRNAs and piRNAs. Non-coding DEGs particularly abundant in the data set were transfer tRNAs (70 DEGs). All tRNAs in this data set were decreased in infected samples compared to non-infected samples, an effect prevented by DMKG supplementation. To verify the depletion of tRNAs in infected samples, we measured the abundance of specific tRNAs in non-infected cells vs cells infected for 48 h. Furthermore, to investigate the potential role of histone hypermethylation, we included samples treated with the demethylase inhibitor JIB-04 at 24 hpi. Total RNA was extracted from uninfected cells and cells infected for 48 h, with or without JIB-04 treatment. Samples were normalized to the 18S rRNA content and analyzed by Northern blot using probes specific for $tRNA^{Gly\text{-}GCC}$ and $tRNA^{Arg\text{-}GCU}$. Probes for U6snRNA and 5S rRNA were used to normalize the signals (Fig. 5D). The quantity of $tRNA^{Gly\text{-}GCC}$ and of $tRNA^{Arg\text{-}GCU}$ were reduced by about 30% in infected cells compared with non-infected cells, confirming that infection leads to a

decrease in tRNA levels. Addition of JIB-04 24 hpi had no significant effect $tRNA^{Gly\text{-}GCC}$ and $tRNA^{Arg\text{-}GCU}$. Thus, while this experiment confirms that tRNA levels diminish during late *C. trachomatis* infection, a causal link with sub-optimal demethylase activities remains to be confirmed.

Shut-down of the inflammatory response to *Chlamydia* infection in the mouse genital tract requires histone demethylase activity.

Our observations in epithelial cells in culture indicated that infected cells were sensitized to JIB-04 with two genes of the innate immune response, CCL20 and sST2, differentially regulated upon JIB-04 treatment. Because this histone demethylase inhibitor showed activity in an *in vivo* model of cancer (22) we postulated that in a mouse model of *Chlamydia* infection JIB-04 may modulate the innate immune response to infection. We used vaginal infection model with the mouse adapted strain, *C. muridarum,* and assessed bacterial burdens and cytokines on day 3 (D3) and D6 of infection (Fig. 6A). The innate response to *C. muridarum* infection in female mice peaks around days 3-4 with robust cytokine and chemokine secretion that quickly decreases by D6 (26). Non-infected animals were included in the trial to control for the effect of peritoneal injections. We focused on sST2 and CCL20, as these two cytokines were found to be sensitive to JIB-04 treatment in epithelial cells (Fig. 5C). We also measured transcript levels of classical markers of the early innate response to infection in the female mouse genital tract: IL-6, TNFα and IL1β. Due to the limited amount of material collected in the vaginal lavages, TNFα and IL1β were not tested at D3.

JIB-04 had no discernable effect on bacterial burden at D3 or D6 of infection (Fig. 6B). At D3, the cytokines tested were increased in infected animals compared to controls except for sST2, which was at the threshold for detection both in infected and non-infected samples and was therefore not investigated further. No difference was seen in the amount of IL6 and CCL20 transcripts in the D3 lavages upon JIB-04 treatment (Fig. 6C). At D6, levels for all transcripts except IL-1β significantly decreased compared to non-infected animals (Fig. 6D). This observation implies that the decrease in cytokine production after D3-4 is not a mere return to basal levels of cytokine synthesis but an anti-inflammatory state regulated by histone modifications. Remarkably, transcriptional shut-down of CCL20, IL-6 and TNFα was mitigated in JIB-04 treated infected animals as their level were similar to basal levels observed in non-infected animals. We conclude from this experiment that peritoneal application of JIB-04 dampened the shut-down of inflammatory signals in the female genital tract, arguing for a role of histone demethylases in the tuning of the innate response to infection.

DISCUSSION

Infection with an intracellular pathogen is expected to challenge the metabolic capacity of its host cell. Here we show that infection of epithelial cells by *C. trachomatis* causes global protein hypermethylation late in infection, including hypermethylation of histone lysine residues. We provide evidence that hypermethylation results from the proliferation of bacteria, whose metabolic activity creates an environment unfavorable to the enzymatic activity of host demethylases. Hypermethylation on H3K4 and H3K9 were detected throughout chromatin, suggesting that hypermethylation occurs randomly. Histone hypermethylation modified the transcriptional response of epithelial cells to infection. In line with the observation that hypermethylation occurred on marks associated with active transcription as much as on marks associated with chromatin silencing, its outcome on gene transcription was gene dependent. Finally, we provide evidence that epigenetic changes involving

histone demethylases from the Jumonji family are implicated in the regulation of the innate inflammatory response to infection in mice.

Hypermethylation of several histone marks during *C. trachomatis* infection was previously documented at a whole cell population level (15). Our analysis by immunofluorescence showed cell to cell variability and combinatorial staining for different marks revealed that cells that displayed a high methylation level for a given mark also displayed hypermethylation for other marks. Hypermethylation occurred late in infection and was most prominent in cells with a high bacterial load and was prevented by antibiotic treatment, indicating that bacterial activity was involved. We excluded a role for Nue, the predicted histone methyl transferase of *C. trachomatis*, as hypermethylation was also observed in cells infected by a mutant strain that did not express Nue. A proteomic analysis of infected cells showed that, in addition to histones, several proteins were hypermethylated consistent with the observation that histone demethylases have multiple substrates (27). Hypermethylated proteins include those implicated in mRNA synthesis and processing, with potential consequences on host gene transcription. Hypermethylation also occurred on cytoplasmic proteins such as tubulin or keratin 18. For the latter, the possibility of methylation at the site we identified had already been reported (28).

The hypermethylation of histones and its correlation with bacterial burdens suggested that infection might create an environment favoring methylation reaction over demethylation. Consistent with this premise, we observed that infected cells were strongly sensitized to the histone demethylase inhibitor JIB-04, indicating that demethylase activity is suboptimal late in infection. Several observations support the hypothesis that the metabolic burden of infection is responsible for the global histone hypermethylation (*i*) histone hypermethylation increased with infection time and positively correlated with bacterial load; (*ii*) histone hypermethylation was partially abolished by providing aKG or Fe(II), co-factors for demethylases of the Jumonji family; and (*iii*) histone H3K9 hypermethylation was prevented by overexpression of the cognate histone demethylase (KDM4A). The last two points suggest that aKG and Fe(II) become limiting late in infection. Indeed, Fe(II) is captured from the host cytoplasm by the bacteria (29). The host responds by enhancing expression of the transferrin receptor (3.3-fold increase of the transcript, Table S3, 5-fold increase of the protein, Table S2) but cytosolic and nuclear Fe(II) concentrations might remain at a suboptimal concentration for demethylase activities. The second metabolite, aKG, represents an entry point into *C. trachomatis* incomplete Krebs cycle (30, 31). A prior metabolomic study did not detect variation in global aKG levels during *C. trachomatis* infection in HeLa cells (32). However, the same study revealed a global increase in succinate and fumarate levels over the course of infection. These two metabolites are competitive inhibitors of the 2-oxoglutarate oxygenase activity carried out by Jumonji C domains (5). Thus, an increase in succinate/fumarate, a decrease in aKG or a combination of both might contribute to the suboptimal histone demethylase activity late in infection. Interestingly, we show here that histone hypermethylation occurs in a context of low SAM concentration, which is required for methylation reactions. The decrease in SAM levels was expected as *Chlamydia* highjack SAM (33). Consistent with low SAM levels, we observed that DNA was slightly hypomethylated late in infection, as previously reported (34). How can protein hypermethylation and DNA hypomethylation be reconciled? Methylation and demethylation reactions depend on the relative affinity of each enzyme for their co-factors and on their respective rates of activities (35). This, together with the difference in turnover between DNA and histone methylation events, could account for the observed differences between DNA and histone methylation levels. In addition, enhanced expression of GADD45 (3.8-fold increase of the transcript, Table S2) during infection might compensate for a potential decrease in initiation of

DNA demethylation by Ten-eleven-translocation (Tet) oxidative demethylases, since GADD45 promotes DNA demethylation downstream of these enzymes (36).

Epigenetic marks govern the accessibility of chromatin. Formaldehyde-assisted isolation of regulatory elements enrichment followed by sequencing (FAIRE-Seq) experiments had shown that the proportion of all differentially accessible regions mapping to promoter regions was at its highest late in Hep2 cells infected with *C. trachomatis*, with the majority of regions showing a reduction in chromatin accessibility (37). Our own ChIP-seq analyzes show that, at least for H3K4 and H3K9, methylation marks are spread throughout chromatin. Since histone methylation can repress or activate gene transcription depending on the mark considered and its position relative to the genetic element the overall effect histone hypermethylation might have on host gene expression was unclear. Transcriptomic analyzes revealed a mitigated effect of hypermethylation with similar proportion of genes differentially up- and downregulated upon DMKG supplementation in infected cells. A discrete set of infection-regulated genes responded strongly to DMKG supplementation (Table S4). DMKG and JIB-04 had opposite effects on the expression of these genes, confirming that histone methylation contributed significantly to the control of their expression late in infection. DMKG-responsive genes in HeLa cells included CCL20/MIP-3α, the ligand for the chemokine receptor CCR6 and sST2 (also known as IL1RL1), a decoy receptor of IL-33 (38, 39). We confirmed that transcripts for CCL20 increased in the acute (D3) phase of the mouse model of genital infection by *C. muridarum*. However, treatment with JIB-03 had no significant effect on this time point, in contrast to what we had observed *in vitro*. Bacterial load in the mouse genital tract was also unchanged by JIB-04 treatment, unlike *in vitro*, indicating that the local concentration of JIB-04 might be sub-optimal. Our data also suggest that cytokine modulation is very dynamic, and it could also be that D3 *in vivo* does not match 48 hpi *in vitro*. At D6, infected mice displayed a strong downregulation in the transcript levels for CCL20, IL6 and TNFα, whose level was below the basal level measured in non-infected animals. The innate response to *Chlamydia* infection is usually studied through the prism of longitudinal studies on vaginal secretions. When cytokines are measured by RT-qPCR in the tissue, non-infected animals are usually not included to reduce animal numbers. This likely explains why, to the best of our knowledge, the strong downregulation of *Chlamydia*-driven inflammation has not been reported before. The decrease in cytokines levels measured at D6 by others (26) went beyond return to basal levels, indicating that it involved strong anti-inflammatory signals. The downregulation of the transcription of CCL20, IL6 and TNFα was less pronounced in JIB-04-treated animals, indicating that the activities of histone demethylases were required to shut-down the acute innate response to infection. Assessing the long-term effect of JIB-04 exposure would necessitate to optimize the formulation and method of delivery of the drug.

Many non-coding RNA were differentially regulated during infection, in a DMKG sensitive manner. We confirmed the decrease in tRNA levels late in infection by Northern blot. The effect of JIB-04 treatment did not reach significance, thus it remains to be determined whether the reduction of tRNA levels is linked to metabolic imbalance and hypermethylation, as suggested by its sensitivity to DMKG supplementation. It should be noted that SAM is a co-factor for post-transcriptional modifications required for tRNA stability (40). Thus, SAM depletion caused by *C. trachomatis* infection might also contribute. In any case, the global decrease in tRNA might contribute to the decrease in host protein synthesis reported in *Chlamydia* infected cells (41).

Our data converge to link protein hypermethylation in infection to the metabolic pressure exerted by bacterial growth. Does it benefit the host or the bacteria? DMKG and JIB-04, which have opposite effects on histone methylation levels, both impaired bacterial growth. Iron supplementation

prevented histone hypermethylation without affecting bacterial growth. These observations indicate that bacterial development occurs regardless of the histone methylation status *in vitro*. However, a more accurate measure of the advantage or disadvantage of histone hypermethylation is arguably the ability of the host to clear the infection without sequelae. The prolongation of pro-inflammatory signals in mice treated with JIB-04 suggests that hypermethylation might lead to increased inflammation-driven tissue damage. The difficulty of JIB-04 delivery to the mouse genital tract precluded a direct evaluation of this hypothesis. Irrespective of the global outcome of histone hypermethylation regarding the host-pathogen warfare, we provide here the first illustration that the metabolic activity of an intracellular bacterium can compromise homeostasis in the host cytoplasm and weight on the host response to infection.

MATERIAL AND METHODS

Cells. HeLa cells (ATCC) and mouse embryonic fibroblasts (MEFs) were grown in Dulbecco's modified Eagle's medium with Glutamax (DMEM, Invitrogen), supplemented with 10 % (v/v) heat-inactivated fetal bovine serum (FBS). Primary epithelial cells were isolated from ectocervix biopsies of female patients after approval by the French Ethical Committee 'CPP Ile de France 1' on May 9, 2016. Approval and authorization of the National Data Protection authority ('Commission Nationale de l'Informatique et des Libertés', CNIL) have been obtained for the research protocol, in compliance with the Helsinki principles. Primary cells were cultivated in keratinocyte serum free medium (KSFM, Thermo Fisher Scientific) containing 50 mg/L of bovine pituitary extract (Thermo Fisher Scientific) and 5 μg/L of epidermal growth factor (EGF) human recombinant (Thermo Fisher Scientific) (16). They were used between passage 3 and 6. All cell cultures were maintained at 37 °C, in 5 % CO_2 atmosphere and were routinely tested for mycoplasma by PCR.

Bacteria. The *C. trachomatis* serovar LGV L2 strain 434 was from ATCC. For IFU measurements and for image analysis, this strain stably transformed with a plasmid expressing the green fluorescent protein (GFP) or mCherry under the control of the *incD* promoter ($L2^{IncD}$GFP and $L2^{IncD}$mCherry) were used, respectively (42). For the experiments with organoids *C. trachomatis* L2 or *C. muridarum* CM006 expressing GFP in p2TK2 or pNigg derived vectors respectively were used (17). For Fig. S1 *C. muridarum* was the MoPn strain provided by Scot Ouellette (University of Nebraska). The *C. trachomatis* serovar LGV L2 strain 434 with an allele in *nuE* leading to a W71* truncation (C to T mutation at position 129786) was obtained by chemical mutagenesis as previously described (19). The resulting rifamycin resistant mutant CTL2M340 was back-crossed with a spectinomycin resistant wild type L2 strain to give rise to the CTL2M340rs59 recombinant strain (referred here as Nue*). Nue* counts 16 single nucleotides polymorphisms (SNPs) compared to the parental strain, which are listed in Table S8. Bacteria were propagated on HeLa cells using standard procedures (43).

Immunofluorescence. Cells (50^4 per well) were seeded in a 24 well-plate on a glass coverslip and infected at MOI=1 the following day. In some experiments, the medium was changed 24 hpi for complete medium supplemented with ferric ammonium citrate (MP Biomedicals #158040 100 mM stock), or dimethyl α-ketoglutarate (DMKG, Sigma #349631, the 7.18 M preparation was adjusted to 2.5 M stock with DMSO, aliquoted and frozen), or JIB-04 (Sigma #SML0808 5 mM stock in DMSO), or doxycycline (Sigma #D3072 10 μg/ml stock in culture medium). Cells were fixed 48 hpi unless otherwise indicated in 4% paraformaldehyde (PFA) 4% sucrose in phosphate buffer saline (PBS) for 20 min, followed with 10 min in 50 mM NH4Cl in PBS, and then washed in PBS. Coverslips were permeabilized

with 0.3% Triton-X100 in PBS for 5 min and washed in PBS. Samples were incubated for 1 hour in primary antibodies diluted in 1mg/ml bovine serum albumin (BSA) 0.01% Tween-20 in PBS, washed 3 times in PBS, and then incubated for 1 hour in secondary antibodies with 0.5 μg/ml 4,6-diamidino-2-phenylindole (DAPI) (Invitrogen). Antibodies used are listed in Table S6. Samples were washed in PBS and then mounted on slides in mowiol. Microscopy was performed on an Axio observer Z1 microscope equipped with an ApoTome module (Zeiss, Germany) and a 20X Apochromat lens. Images were taken with an ORCAflash4.OLT camera (Hamamatsu, Japan) using the ZEN software from Zeiss.

Image analysis and quantification. (i) *on cells infected with non-fluorescent bacteria* (Fig. 1 and 2A). Image analysis was performed with Fiji (44). We used the Trainable Weka segmentation plugin (45) to generate a probability map for the nucleus signal, used in turn to produce a mask of the nuclei with a threshold value of 0.75. The mask was corrected by morphological closing with a radius of 2 pixels. Incorrectly merged nuclei were separated using the Distance Transform Watershed operation. Finally, we used TrackMate (46) to remove spurious objects (corpses) by filtering them based on their areas and exported all measurements to a CSV file. A Fiji script that wraps up all the steps can be found on gitlab. Intensity values in the green and far red channel were extracted for each nuclei, from non-infected and infected samples, in at least 3 different images. The mean value of intensity for a given histone mark in non-infected samples was calculated. Nuclei whose intensity was 2-fold or more above this value were counted as positive. Z-normalization was applied to the intensity scores before measuring correlation between the marks (47) (ii) *on cells infected with fluorescent bacteria* (all other Fig.) Image analysis was performed with Fiji (44), the different steps described below were automatically performed using a Fiji macro script. Cell nuclei and inclusions appeared in the uv/DAPI channel (DNA stain) while only inclusions appeared in the red/mCherry channel (mCherry expressing bacteria). A median filter of radius 2 was applied to both channels for noise removal. “Triangle” and “Huang” automatic threshold methods were respectively used on mCherry and DAPI channels to create binary masks. The mCherry mask was subtracted from the DAPI mask, resulting in a binary mask corresponding to cells nuclei. The FIJI functions “Erode”, “Dilate”, “Fill Holes” and “Watershed” were successively applied to the resulting mask for nuclei individualization. The FIJI functions “Erode”, “Dilate” 2 times and “Watershed” were successively applied to the inclusion mask to individualize inclusions and dilate them by one pixel to create an overlap with the nuclei next to inclusions. Regions of interest (ROI) corresponding to inclusions were defined on the inclusions mask using “Analyze Particles” function with “Size” parameter set to “30-Inf”. ROI corresponding to nuclei were defined on the nuclei mask using “Analyze Particles” function with “Size” parameter set to “50- 500” and “Exclude on edges” option on. For each nuclei ROI, the macro checked each inclusion ROI one by one to see if there was an overlap with the nuclei ROI. This was done by selecting the intersection of both ROI (“AND” function of the ROI Manager) and by checking if it was not empty (selectionType() > -1). Nuclei were considered as from an infected cell if they were overlapping with at least one inclusion. For Fig. 2D, the overlap area was measured, and nuclei were associated with the inclusion they were overlapping the most with. The mean intensity in each channel was measured for each nucleus and inclusion. Finally, for each field, three composite pictures of DAPI and mCherry channels were saved, displaying either inclusions, infected or non-infected nuclei segmentation for postprocessing verification. The mean value of intensity for a given histone mark in non-infected samples was calculated. Nuclei whose intensity was greater than two times this value were counted as positive. Positive nuclei from non-infected cells were manually double checked and corrected as nuclei from infected cells if they had been misclassified by the automated procedure.

Organoid culture and imaging. Murine endometrial organoids were generated as previously described from C57BL/6J (Jackson Laboratory, strain no. 000664) (17). Bacteria were diluted in phosphate-buffered saline to a final concentration of 5 x 10^6 IFU, vortexed for 15 seconds, and pipetted into a borosilicated capillary glass needle. Organoids were microinjected using an Eppendorf FemtoJet 4x using a steep vertical angle and only punctured once and refed with media containing 10 ug/mL gentamicin one hour after injection. At the indicated timepoint, organoids were washed with warm PBS, fixed with 3% warm paraformaldehyde for 20 minutes, and resuspended in 0.5 mL 0.25% ammonium chloride. Organoids were centrifuged at 600 x *g* for 5 minutes, resuspended in PBS containing 2% BSA (Fraction V; Equitech-Bio) and 0.1% triton X-100 (Sigma), and incubated on a rocker at 25 °C. The organoids were centrifuged at 600 x *g* for 5 min and incubated with rabbit anti-H3K9me3 (1:50) overnight at 4 °C. Organoids were washed once with 2% BSA, centrifuged at 600 x *g* for 5 min, and incubated with anti-rabbit conjugated to AlexFluor 647 (1:1,000) and Hoechst (2 ug/mL) for 1.5 hours at 25 °C. Organoids were centrifuged at 600 x *g* for 5 minutes, resuspended in Vectashield (Vector Labs; H-1000), pipetted onto a glass slide and overlaid with a coverslip. Organoids (9 organoids for infections with *C. trachomatis* and 7 for *C. muridarum*) were imaged using an inverted microscope (TI2-E; Nikon Instruments) equipped with an ORCA Flash 4.0 V3 sCMOS camera (Hamamatsu), SOLA solid-state white illumination (Lumencor) and acquired using a 20x Plan Apochromatic NA 0.75 air objective with the NIS-Elements Software (Nikon). 3D reconstructions were generated in ImageJ (NIH) and the nuclei were segmented using auto local thresholding and the watershed algorithms. The mean intensity in infected cells and neighboring, uninfected cells was measured, plotted and analyzed in R Studio. Statistical analysis was performed using a Welch's t-test.

Proteomic analyses. 35 mm dishes were plated with 400.000 HeLa cells and infected or not the following day with *C. trachomatis* L2 at MOI=2. Forty-eight hours later the cells were collected and resuspended in Tris 100mM, 8M urea pH 7.5. Biological triplicates were prepared. Proteins were reduced using 5 mM TCEP for 30 min at room temperature. Alkylation of the reduced disulfide bridges was performed using 10 mM iodoacetamide for 30 min at room temperature in the dark. Proteins were then digested in two steps, first with 1 µg r-LysC Mass Spec Grade (Promega) for 4 h at 30°C and then samples were diluted to 1.8 M urea with 100 mM Tris HCl pH 8.5 and 1 µg Sequencing Grade Modified Trypsin was added for the second digestion overnight at 37°C. Proteolysis was stopped by adding formic acid (FA) at a final concentration of 5%. The resulting peptides were desalted on Stage Tip (48) prepared with Empore 3M C18 material (Fisher Scientific). Peptides were eluted using 50 % acetonitrile (ACN), 0.1 % formic acid (FA). Peptides were concentrated to dryness and resuspended in 2 % ACN/0.1 % FA just prior to LC-MS injection.

LC-MS/MS analysis was performed on a Q Exactive™ Plus Mass Spectrometer (Thermo Fisher Scientific) coupled with a Proxeon EASY-nLC 1200 (Thermo Fisher Scientific). One µg of peptides was injected onto a home-made 32 cm C18 column (1.9 µm particles, 100 Å pore size, ReproSil-Pur Basic C18, Dr. Maisch GmbH, Ammerbuch-Entringen, Germany). Column equilibration and peptide loading were done at 900 bars in buffer A (0.1 % FA). Peptides were separated with a multi-step gradient from 3 to 6 % buffer B (80% ACN, 0.1% FA) in 5 min, 6 to 31 % buffer B in 130 min, 31 to 62 % buffer B in 30 min at a flow rate of 250 nL/min. Column temperature was set to 60°C. MS data were acquired using Xcalibur software using a data-dependent method. MS scans were acquired at a resolution of 70,000 and MS/MS scans (fixed first mass 100 m/z) at a resolution of 17,500. The AGC target and maximum injection time for the survey scans and the MS/MS scans were set to 3E6, 20ms and 1E6, 60ms respectively. An automatic selection of the 10 most intense precursor ions was activated (Top 10) with

a 30 s dynamic exclusion. The isolation window was set to 1.6 m/z and normalized collision energy fixed to 27 for HCD fragmentation. We used an underfill ratio of 1.0 % corresponding to an intensity threshold of 1.7E5. Unassigned precursor ion charge states as well as 1, 7, 8 and >8 charged states were rejected and peptide match was disable.

Protein identification. Acquired Raw data were analyzed using MaxQuant software version 1.6.6.0 using the Andromeda search engine (49). The MS/MS spectra were searched against the *Chlamydia trachomatis* serovar L2-434-Bu and the Homo Sapiens Uniprot reference proteome database (884 and 79057 entries respectively). All searches were performed with oxidation of methionine, mono- and di-methylation of lysine and arginine, trimethylation of lysine, and acetylation of lysine and protein N-terminal as variable modifications and cysteine carbamidomethylation as fixed modification. Trypsin was selected as protease allowing for up to two missed cleavages. The minimum peptide length was set to 5 amino acids and the peptide mass was limited to a maximum of 8,000 Da. One unique peptide to the protein group was required for the protein identification. The main search peptide tolerance was set to 4.5 ppm and to 20 ppm for the MS/MS match tolerance. Second peptides was enabled to identify co-fragmentation events and match between runs option was selected with a match time window of 0.7 min over an alignment time window of 20 min. The false discovery rate (FDR) for peptide and protein identification was set to 0.01.

Statistical analysis on proteomics data was based on the comparison of intensities between biological conditions. Proteins identified as reverse hits or potential contaminants were first removed from the analysis. Intensities associated with at least one unique peptide were kept for further statistics. Additionally, only proteins with at least two intensity values in one of both conditions were kept to ensure a minimum of replicability. Next, intensities were log2-transformed. They were normalized so that the intensities of human proteins are centered in each sample on the mean of the medians of the human protein intensities across all samples. This normalization was carried out to ensure that the intensities in each sample corresponded to a same global level of the host proteins. Proteins without any intensity value in one of both conditions have been considered as proteins quantitatively present in a condition and absent in the other. They have, therefore, been set aside and considered as differentially abundant proteins. Next, missing values of the remaining proteins were imputed using the impute.mle function of the R package imp4p (50). Statistical testing was conducted using limma t-tests thanks to the R package limma (51). The FDR control was performed using an adaptive Benjamini–Hochberg procedure on the resulting p-values thanks to the function adjust.p of R package cp4p using the robust method to estimate the proportion of true null hypotheses among the set of statistical tests (52). The proteins associated to an absolute log2(fold-change) superior to 1 and adjusted p-values inferior to a FDR level of 1% have been considered as significantly differentially abundant proteins.

Statistical analysis of modified peptides. We searched for mono-, di- or tri-methylations on lysine or arginine residues. Some modifications were identified through mass differences in MS1 spectra, without precise localization on the peptide. Others have been pinpointed on their respective peptides using MS/MS spectra with localization probabilities exceeding 0.75 as determined by MaxQuant. For statistical analyses, raw intensities of all identified modified peptides in the experiments were log2-transformed. Subsequently, they were normalized by median centering within the biological conditions (infected or not infected) to account for potential shifts in peptide median signals between conditions. Missing values were then imputed by condition using the impute.mle function from the R package imp4p. Standard t-tests were employed to examine whether the fold-changes of modified peptides significantly differed from 0 between conditions. Furthermore, ANOVA contrast analyses

were conducted to identify modified peptides with fold-changes significantly different from those of the unmodified proteins to which they belong as explained in (53).

Nuclei isolation and measure of DNA methylation. 35 mm dishes were seeded with 4x10^5 HeLa cells. Cells were infected or not at MOI 2 with *C. trachomatis* LGV L2. Forty-eight hpi, cells were washed in PBS and detached in PBS-EDTA, centrifuged for 5 min at 400 x*g* and resuspended in 344 ml of hypotonic buffer (10 mM Tris pH 7.65, 1.5 mM MgCl2, 10 mM KCl, 0.2% NP-40, 0.6 mM phenylmethanesulfonyl (PMSF), 1X Protease inhibitor cocktail (Sigma)). Volume was adjusted to about 1 ml by adding PBS, cells were then lysed using a Dounce homogenizer (20 up and down), and then 96 µl of Sucrose buffer (20 mM Tris-HCl pH 7.65, 15 mM KCl, 60 mM NaCl, 0.34 M sucrose, 150 mM spermine (Merck S4264), 50 mM spermidine (Merck S0266), 0.6 mM PMSF, 1X Protease inhibitor cocktail (Sigma)) was added to the samples. Samples were centrifuged for 5 min at 500 x*g*, supernatants were discarded and the pellets frozen. Genomic DNA was extracted with RNase A and digested with the kit Nucleoside digestion mix of NEB (M0649S) according to the manufacturer's protocol. The reaction was processed for LC-MS/MS analysis. Analysis of total 5-methyl-2'-deoxycytidine (5-mdC) concentrations was performed using a Q exactive mass spectrometer (Thermo Fisher Scientific), equipped with an electrospray ionization source (H-ESI II Probe) coupled with an Ultimate 3000 RS HPLC (Thermo Fisher Scientific). Digested DNA was injected onto a Thermo Fisher Hypersil Gold aQ chromatography column (100 mm x 2.1 mm, 1.9 µm particle size) heated at 30 °C. The flow rate was set at 0.3 mL/min and run with an isocratic eluent of 1% acetonitrile in water with 0.1 % formic acid during 10 min. Parent ions were fragmented in positive ion mode with 10 % normalized collision energy in parallel-reaction monitoring (PRM) mode. MS2 resolution was 17,500 with an AGC target of 2e5, a maximum injection time of 50 ms and an isolation window of 1.0 m/z. The inclusion list contained the following masses: dC (228.1), 5-mdC (242.1). Extracted ion chromatograms of base fragments (±5ppm) were used for detection and quantification (112.0506 Da for dC; 126.0662 Da for 5-mdC). Calibration curves were previously generated using synthetic standards in the ranges of 0.2 to 50 pmoles injected for dC and 0.02 to 10 pmoles for 5mdC. Results are expressed as a % of total dC.

SAM measurement. For each condition, a 10 cm dish was seeded with 2.5 million HeLa cells. Cells were infected or not at MOI 2 with C. trachomatis LGV L2. Forty hpi, nuclei were isolated as described above. The samples were divided in 8 aliquots and centrifuged at 500 x*g* for 5 minutes. The pellet (nuclei) was resuspended in 40 ul of CM buffer from the Mediomics Bridge-It® SAM fluorescence assay (Gentaur) (2 aliquots) or of urea buffer (30 mM Tris, 150 mM NaCl, 8 M urea, 1 % SDS, pH=8.0) (1 aliquot) to determine protein concentration using a BCA protein assay kit (Pierce 23225). Aliquots were normalized to equal protein concentrations in CM buffer, diluted 1:4 in CM buffer and incubated for 1 h at 24 °C with vigorous shaking. Samples were centrifuged for 5 min at 16,000 x*g*. The supernatant was diluted 1:5 in Buffer S, mixed and 20 ul of the mix was deposited on one Optiplate (Perkin Elmer #6005270) in duplicates. 80 ul of Reaction Buffer was added to each well. The reaction was incubated for 40 min at room temperature before reading fluorescence resonance energy transfer (FRET) on a FLUOStar Omega with filters (485-12 excitation 540nm-10 emission, 485-12 excitation 660-10 emission). SAM concentrations in test samples are then determined using a SAM standard curve.

Progeny assays. Hela cells (10^5) were seeded in a 24-well plate. The next day cells were infected with $L2^{IncD}$GFP bacteria at a MOI = 0.15. Twenty-for post infection, the medium was replaced with fresh medium supplemented with the indicated drug, or left unchanged, with the addition of DMSO in the well if the drug was dissolved in DMSO. Cells were detached 48 hpi, lysed using glass beads and the

supernatant was used to infect new HeLa cells plated the day before (100 000 cells/well in a 24-well plate), in serial dilution. The next day, 3 wells per condition with an infection lower than 30 % (checked by microscopy) were detached and fixed as described above, before analysis by flow cytometry and determination of the bacterial titer. Acquisition was performed using a CytoFLEX S (Beckman Coulter) and 50 000 events per sample were acquired and then analyzed using FlowJo (version 10.0.7).

Transfections. One day after being seeded in a 24 well-plate (10^5 cells/well) in 500 µL of complete medium transfection mix was added to cells (50 µL of Jetprime buffer (Polyplus), 0.5 µg of DNA, and 3 µL of Jetprime transfection reagent (Polyplus) per well. After 3h, the medium was changed for new complete medium containing mCherry-bacteria at MOI=0.5. Plasmids used were coding for HA-tagged KDM4A/JMJD2A (Addgene #24180) or for an irrelevant HA-tagged construct HA-Tsg5' as negative control (24).

Chromatin immunoprecipitation. Four 15 cm culture dishes were seeded with 6x10^6 cells) and half were infected the day after at MOI=2. Forty-eight h later cells were rinsed twice in PBS and fixed by adding 15 ml of fixation medium prewarmed to 37 °C (15 mM NaCl, 0.15 mM EDTA, 0.075 mM EGTA, 0.015 mM HEPES in DMEM pH8.0. Formaldehyde (Sigma F-8775) was added to the prewarmed medium just prior to the fixation step to the final concentration of 1%. Cells were rocked gently at room temperature, afterwards formaldehyde was quenched by adding glycine drop by drop from a 1.06M stock prepared fresh to a finale concentration of 0.125 M. Quenching was pursued for 5 min with gentle rocking, the cells were rinsed twice with PBS, scraped using a soft silicon scraper and transferred to a 15 ml conical tubes on ice, pooling the two identical plates together. Cells were centrifuged at 400 x*g* for 10 min at 4 °C, the pellet was resuspended in 10 ml cold PBS, centrifuged again. The pellet was resuspended in 1 ml of cold PBS and centrifuged, the supernatant was discarded and the pellet frozen at – 80 °C. Pelets were resuspended in lysis buffer (50 mM HEPES (pH 7.5), 140 mM NaCl, 1 mM EDTA (pH 8), 10% glycerol, 0.5% NP-40, 0.25% Triton X100) and incubated 10 min at 4°C. After centrifugation (300 x g, 5 min, 4°C) the supernatant was discarded, the pellet resuspended in buffer (200 mM NaCl, 1 mM EDTA (pH 8), 0.5 mM EGTA (pH 8), 10 mM Tris-HCl (pH 8) and FPIC (Fast Protease Inhibitors Cocktail; Sigma-Aldrich; #S8830-20TAB) and incubated 10 min at 4 °C. After centrifugation the supernatant was discarded and the pellet resuspended in low-SDS buffer (50 mM Tris-HCl (pH 8), 0.1% SDS, 0.95% NP-40, 0.1% NaDoC, 10 mM EDTA (pH 8), 150 mM NaCl and FPIC) for sonication for 4 min (4 x (30 s ON, 30 s OFF)) (Bioruptor, Diagenode), yielding genomic DNA fragments with a bulk size of 150–500 bp. 1% of chromatin extracts were taken aside for inputs. Chromatin corresponding to 5 µg of DNA was incubated with 2 µg of anti-H3K4me3 (Diagenode; Cat#: C15410003) or anti-H3K9me3 (Diagenode; Cat#: C15410193) antibodies overnight at 4◦C. The DNA-protein-antibody complexes were captured by DiaMag protein A-coated magnetic beads (Diagenode; Cat#: C03010020) by incubating at 4°C for 2 h. Magnetic beads were then washed with low-salt buffer (20 mM Tris-HCl (pH 8), 0.1% SDS, 1% Triton X100, 2 mM EDTA (pH 8), 150 mM NaCl and FPIC) and high-salt buffer (20 mM Tris–HCl (pH 8), 0.1% SDS, 1% Triton X100, 2 mM EDTA (pH 8), 500 mM NaCl and FPIC). DNA was eluted with TE buffer (100 mM Tris-HCl (pH 8), 1% SDS, 1 mM EDTA (pH 8)) from the beads overnight, and then reverse cross-linked with 1 µl of RNase A (10 µg/ml; Sigma-Aldrich; Cat#: R4642), followed by Proteinase K digestion (5 µl of 20 mg/mL; Sigma-Aldrich; Cat#: P2308) during 2 h; inputs corresponding to 1% of IP were reverse cross-linked in the same conditions. DNA was purified using MinElute PCR Purification Kit (Qiagen; Cat#: 28004). 2 µl of input and ChIP were loaded on High Sensitivity D5000 ScreenTape (Agilent Technologies #5067-5592) with 2 µl of reagent (#5067-5593) (Fig. S4A). Libraries were prepared using the MicroPlex Library Preparation Kit v3 (Diagenode)

according to the manufacturer's protocol. In brief, 1 to 25 ng were used as input material. After adapters ligation, fragments were amplified with Illumina primers for 10 cycles. Libraries were purified using AMPure XP beads protocol (Beckman Coulter, Indianapolis, IN) and quantified using the Qubit fluorometer (Thermo Fisher Scientific). Libraries' size distribution was assessed using the Bioanalyzer High Sensitivity DNA chip (Agilent Technologies). Libraries were normalized and pooled at 2 nM and spike-in PhiX Control v3 (Illumina) was added. Sequencing was done using a NextSeq 500 instrument (Illumina) in paired-end mode (2x40 cycles) and a NextSeq 2000 instrument (Illumina) in paired-end mode (2x50 cycles). After sequencing, a primary analysis based on AOZAN software (ENS, Paris, France) (54) was applied to demultiplex and control the quality of the raw data (based on bcl2fastq v2.20, bcl-convert v4.1.5 and FastQC modules / v0.11.5).

ChIP-seq datasets were analyzed under the Galaxy platform (https://usegalaxy.eu) (55). The Quality of raw data has been evaluated with FastQC (Galaxy Version 0.74) (https://www.bioinformatics.babraham.ac.uk/projects/fastqc/). Poor quality sequences and adapters have been trimmed or removed with Trimmomatic (Galaxy Version 0.23.2) software (56) to retain only paired reads of 40 bp with Phred score >20. Reads were mapped to the reference genomes (GRCh38) using Bowtie2 (Galaxy Version 2.5.0) (57) to generate BAM files. Duplicates were removed by using the Picard tool MarkDuplicates (Galaxy Version 2.18.2.4). Narrow and broad peaks were called with MACS2 (Galaxy Version 2.2.7.1) (58) using the input as control, FDR ≤ 0.05. Differential binding analysis of ChIP-Seq peak data was performed using DiffBind (Galaxy Version 2.10.0) (59). Peak annotation was performed by using the ChIPseeker R package (60) and Bedtools intersect (Galaxy Version 2.28.0) (61) to annotate peaks according to their chromatin feature with genome segmentation data from ENCODE (62, 63). The Gene ontology enrichment analysis was performed with the clusterProfiler R package (64). The significant GO categories were identified with Benjamini-Hochberg adjusted p-value ≤ 0.05.

Microarray A 6-well plate was seeded with 200,000 HeLa cells per well. The following day, cells were infected with *C. trachomatis* LGV L2 at MOI=2. 24 hpi, the media was replaced by complete medium supplemented with 5 mM DMKG or left unchanged with addition of an equal volume of DMSO. Forty-eight hpi RNA was harvested using the RNeasy kit (Qiagen), and their quality was analyzed using the BioAnalyzer (Agilent). Transcriptome analysis was done using the GeneChip Human Transcriptome Array 2.0 for in combination with the GeneChip WT PLUS Reagent kit (Applied Biosystems). 33,3ng total RNA was used as input for the analysis that was done according to the manufacturer's guidelines. In brief, double-stranded cDNA is first synthesized using random primers and then used as template for in vitro transcription (IVT) that produces amplified amounts of antisense mRNA (cRNA). The cRNA is used as input for a second round of first strand cDNA synthesis, producing single stranded sense cDNA. After fragmentation and end-labeling the targets are hybridized to single sample GeneChip cartridge arrays that are stained and washed on a GeneChip Fluidics Station 450 and scanned on a GeneChip scanner 3000 7G. Cell files containing the probe cell intensity data generated by the scanner is imported into the Expression Console Software 4.0.1 (Thermo Fisher Scientific) for data analysis. Expression values corresponds to Robust Multiarray Average (RMA) normalized probe set intensities.

RT-qPCR and qPCR. Total RNAs from cells in culture were isolated 48 hpi with the RNeasy Mini Kit (Qiagen) with DNase treatment (DNase I, Roche). RNA concentrations were determined with a spectrophotometer NanoDrop (Thermo Fisher Scientific) and normalized to equal contents. Reverse transcription (RT) was performed using the M-MLV Reverse Transcriptase (Promega). Total RNAs and genomic DNA from lavage fluids and mouse tissue homogenate were extracted using AllPrep® DNA/RNA Micro Kit (Qiagen, #80284). The tissue homogenate was prepared by disrupting frozen tissue

in pre-chilled Lysing Matrix D 2 mL tube (MP Biomedicals) containing 400 μl PBS using a Precellys 24 tissue homogenizer (Bertin, Germany). After pelleting the tissue debris (14,000 ×*g*, 2 min), 200 μl of the supernatant was used to extract RNA and genomic DNA. Quantitative PCR (qPCR) was undertaken on DNA or on complementary DNA (cDNA) with LightCycler 480 system using LightCycler 480 SYBR Green Master I (Roche). Data were analyzed using the ΔΔCt method with the *actin* gene as a control gene (65). Each RT-qPCR experiment was performed in duplicate and repeated at least three times. Primer used are listed in Table S7.

tRNA quantification. tRNA were extracted and analyzed by northern blot as described (66) with the exception that in some cases samples were run on a 6% PAGE (instead of 8%) to get better separation between the 5S rRNA and the U6 snRNA.

Infection in mice. The experiments were performed in accordance with the French national and European laws regarding the protection of animals used for experimental and other scientific purposes. The study was approved by the ethics committee of Institut Pasteur (approval N° dap210086). Female c57BL/6J mice aged 6-7 weeks were purchased from Charles River Laboratories (France) and housed in the animal facility at Institut Pasteur. JIB-04 was synthesized as described (22). All animals were treated with 2.5 mg of medroxyprogesterone (Depo-provera-SC®, Pfizer) 7 days prior to infection to synchronize their menstrual cycle. Vaginal lavages were conducted the day prior to infection twice with 50 μl PBS each time by pipetting up and down several times followed with swabbing to remove the mucus. On day 0, the animals were anesthetized by intramuscular injection of Ketamine/Xylazine in PBS before intra-peritoneal (i.p.) injection of JIB-04 (100 mg/kg body weight) resuspended in 300 μl sesame oil (Sigma #3547), control animals were injected with sesame oil only. $2x10^5$ IFUs of *C. muridarum* resuspended in 5 μl of sucrose-phosphate-glutamic acid buffer (SPG: 10 mM sodium phosphate [8 mM Na2HPO4- 2 mM NaH2PO4], 220 mM sucrose, 0.50 mM l-glutamic acid) were introduced in the vagina of mice, control mice were treated with the same volume of SPG alone. Additional doses of JIB04 or sesame oil were injected i.p. at D2 and D4. A vaginal lavage was performed at D3 and two washes were pooled and frozen immediately into liquid nitrogen. Upon D6 the animals were sacrificed by cervical dislocation. The lower (vagina and cervix) genital tracts were excised and frozen immediately into liquid nitrogen.

Statistical analyses. The R environment v4.1.2 was used for analysis of tRNA quantification and qPCR (67). Data were not averaged prior analysis. For tRNA quantification shown in Fig 5D, band intensities were measured in each well of northern blot pictures and the log2 of (band of interest intensity / control band intensity) was computed, with band of interest being either GlyGCC or ArgGCU tRNA, and with control band being either U6 or 5S rRNA. Then, data were fitted to a mixed linear model that included the condition and the technical replicates as random covariate (i.e., band intensity ~ condition + (1|replicate)). For qPCR analysis (Fig 5C and Fig6C-D), a variation of the ΔΔCt method (gene of interest versus actin) (65) that keeps the technical replicate variations was applied. These values were fitted to a mixed linear model that included the treatment and the technical replicates as random covariate (i.e., ΔΔCt2 ~ treatment + (1|replicate) in Fig 5 C and ΔCt2 ~ treatment + (1|replicate) + (1|treatment:replicate) in Fig 6 C-D to take nesting into account). Then, contrasts were performed with the emmeans() function of the emmeans package. Statistical significance was set to $P \leq 0.05$. In each figure, type I error was controlled by correcting the p values according to the Benjamini & Hochberg method ("BH" option in the p.adjust() function of R). The nature of the statistical tests used in other figures are provided in the respective legend.

ACKNOWLEDGEMENTS

We thank Béatrice Niragire, Klementina Borovnik and Valentin Petit for technical assistance, Drs MS Phan and JY Tinevez for the pipeline of analysis of images of infected cells with non-fluorescent inclusions, Drs Mélanie Hamon, Paola Arimondo, Sophie Polo and Mikhail D. Magnitov for discussion and reagents.

Funding

Agence Nationale pour la Recherche 20-PAMR-0011 TheraEPI (AS, MM)

Fondation ARC pour la recherche sur le Cancer (AS)

Institut national du cancer INCA_ 16719 (AS)

Institut Pasteur (YW, GM, QGG, MD, MM, FB)

Centre National de la Recherche Scientifique (AS, SP, SA)

Pasteur - Paris University (PPU) International PhD Program (CIC)

DIM1Health 2019 grant from the Région Ile de France to the project EpiK (LC/MS-MS equipment).

Collaborative Research Centre 992 Medical Epigenetics DFG grant SFB 992/1 2012 (The Galaxy server)

German Federal Ministry of Education and Research (BMBF grants 031 A538A/A538C RBC, 031L0101B/031L0101C de.NBI-epi, 031L0106 de.STAIR (de.NBI))

Author contribution

Conceptualization: CIC, AS
Investigation: CIC, FL, YW, LD, SP, AGT, LB, MD, LDM, FB
Data analysis: CIC, FL, LD, GV, AGT, QGG, MM, FB, GM, AS
Visualization: CIC, FL, LD, AS
Resources: YW, EM
Funding acquisition : LRP, SA, EDM, RHV, AS
Writing—original draft: CIC, FL, LD, GV, MD, QGG, AS
Writing—review & editing: AGT, SA, RHV, AS

Competing interests: Authors declare that they have no competing interests.

REFERENCES

1. K. Luger, M. L. Dechassa, D. J. Tremethick, New insights into nucleosome and chromatin structure: an ordered state or a disordered affair? *Nature Rev. Mol. Cell Biol.* **13**, 436-447 (2012).

2. X. Su, K. E. Wellen, J. D. Rabinowitz, Metabolic control of methylation and acetylation. *Curr. Opin. Chem. Biol.* **30**, 52-60 (2016).

3. R. Boon, G. G. Silveira, R. Mostoslavsky, Nuclear metabolism and the regulation of the epigenome. *Nature metabolism* **2**, 1190-1203 (2020).

4. S. L. Accari, P. R. Fisher, "Emerging Roles of JmjC Domain-Containing Proteins" in International Review of Cell and Molecular Biology, K. W. Jeon, Ed. (Academic Press, 2015), vol. 319, pp. 165-220.

5. M. Xiao *et al.*, Inhibition of α-KG-dependent histone and DNA demethylases by fumarate and succinate that are accumulated in mutations of FH and SDH tumor suppressors. *Genes Dev.* **26**, 1326-1338 (2012).

6. J. S. Shapiro *et al.*, Iron drives anabolic metabolism through active histone demethylation and mTORC1. *Nat. Cell Biol.* **25**, 1478-1494 (2023).

7. Y. Jiang *et al.*, Iron-dependent histone 3 lysine 9 demethylation controls B cell proliferation and humoral immune responses. *Nature Comm.* **10**, 2935 (2019).

8. M. A. Reid, Z. Dai, J. W. Locasale, The impact of cellular metabolism on chromatin dynamics and epigenetics. *Nat Cell Biol* **19**, 1298-1306 (2017).

9. K. A. Krautkramer *et al.*, Diet-Microbiota Interactions Mediate Global Epigenetic Programming in Multiple Host Tissues. *Mol. Cell* **64**, 982-992 (2016).

10. R. G. Nichols, E. R. Davenport, The relationship between the gut microbiome and host gene expression: a review. *Hum. Genet.* **140**, 747-760 (2021).

11. Y. Zhao, C. Wang, A. Goel, Role of gut microbiota in epigenetic regulation of colorectal Cancer. *Biochimica et biophysica acta. Reviews on cancer* **1875**, 188490 (2021).

12. Y. Abu Kwaik, Nutrition-based evolution of intracellular pathogens. *Environmental microbiology reports* **7**, 2-3 (2015).

13. R. C. Brunham, J. Rey-Ladino, Immunology of *Chlamydia* infection: Implications for a *Chlamydia trachomatis* vaccine. *Nat. Rev. Immunol.* **5**, 149-161 (2005).

14. Y. M. AbdelRahman, R. J. Belland, The chlamydial developmental cycle. *FEMS Microbiol. Rev.* **29**, 949-959 (2005).

15. C. Chumduri, R. K. Gurumurthy, P. K. Zadora, Y. Mi, T. F. Meyer, *Chlamydia* infection promotes host DNA damage and proliferation but impairs the DNA damage response. *Cell Host Microbe* **13**, 746-758 (2013).

16. C. Tang *et al.*, Primary ectocervical epithelial cells display lower permissivity to *Chlamydia trachomatis* than HeLa cells and a globally higher pro-inflammatory profile. *Sci Rep* **11**, 5848 (2021).

17. L. Dolat, R. H. Valdivia, An endometrial organoid model of interactions between Chlamydia and epithelial and immune cells. *J. Cell Sci.* **134** (2021).

18. M. E. Pennini, S. Perrinet, A. Dautry-Varsat, A. Subtil, Histone methylation by NUE, a novel nuclear effector of the intracellular pathogen *Chlamydia trachomatis*. *PLoS Pathog* **6**, e1000995 (2010).

19. M. Kokes *et al.*, Integrating chemical mutagenesis and whole-genome sequencing as a platform for forward and reverse genetic analysis of Chlamydia. *Cell Host Microbe* **17**, 716-725 (2015).

20. D. Husmann, O. Gozani, Histone lysine methyltransferases in biology and disease. *Nature Structural & Molecular Biology* **26**, 880-889 (2019).

21. A. Maiques-Diaz, T. C. P. Somervaille, LSD1: biologic roles and therapeutic targeting. *Epigenomics* **8**, 1103-1116 (2016).

22. L. Wang *et al.*, A small molecule modulates Jumonji histone demethylase activity and selectively inhibits cancer growth. *Nature Comm.* **4**, 2035 (2013).

23. J. R. Whetstine *et al.*, Reversal of histone lysine trimethylation by the JMJD2 family of histone demethylases. *Cell* **125**, 467-481 (2006).

24. F. Vromman, S. Perrinet, L. Gehre, A. Subtil, The DUF582 Proteins of Chlamydia trachomatis Bind to Components of the ESCRT Machinery, Which Is Dispensable for Bacterial Growth In vitro. *Front Cell Infect Microbiol* **6**, 123 (2016).

25. O. Rostan *et al.*, Crucial and diverse role of the interleukin-33/ST2 axis in infectious diseases. *Infect. Immun.* **83**, 1738-1748 (2015).

26. M. Nagarajan Uma *et al.*, MyD88 Deficiency Leads to Decreased NK Cell Gamma Interferon Production and T Cell Recruitment during Chlamydia muridarum Genital Tract Infection, but a Predominant Th1 Response and Enhanced Monocytic Inflammation Are Associated with Infection Resolution. *Infect. Immun.* **79**, 486-498 (2011).

27. J. Kuwik *et al.*, Activity Guided Azide-methyllysine Photo-trapping for Substrate Profiling of Lysine Demethylases. *J. Am. Chem. Soc.* **145**, 21066-21076 (2023).

28. K.-H. Jang *et al.*, Liver disease–associated keratin 8 and 18 mutations modulate keratin acetylation and methylation. *The FASEB Journal* **33**, 9030-9043 (2019).

29. N. D. Pokorzynski, C. C. Thompson, R. A. Carabeo, Ironing Out the Unconventional Mechanisms of Iron Acquisition and Gene Regulation in Chlamydia. *Front Cell Inf Microbiol* **7** (2017).

30. R. S. Stephens *et al.*, Genome sequence of an obligate intracellular pathogen of humans: *Chlamydia trachomatis*. *Science* **282**, 754-755 (1998).

31. A. Mehlitz *et al.*, Metabolic adaptation of *Chlamydia trachomatis* to mammalian host cells. *Mol. Microbiol.* **103**, 1004-1019 (2017).

32. M. Rother *et al.*, Combined Human Genome-wide RNAi and Metabolite Analyses Identify IMPDH as a Host-Directed Target against Chlamydia Infection. *Cell Host Microbe* **23**, 661-671.e668 (2018).

33. R. Binet, R. E. Fernandez, D. J. Fisher, A. T. Maurelli, Identification and Characterization of the Chlamydia trachomatis L2 S-Adenosylmethionine Transporter. *mBio* **2** (2011).

34. E. R. Bryan *et al.*, DNA damage contributes to transcriptional and immunological dysregulation of testicular cells during Chlamydia infection. *Am. J. Reprod. Immunol.* **86**, e13400 (2021).

35. M. S. Islam, T. M. Leissing, R. Chowdhury, R. J. Hopkinson, C. J. Schofield, 2-Oxoglutarate-Dependent Oxygenases. *Annu. Rev. Biochem.* **87**, 585-620 (2018).

36. Z. Li *et al.*, Gadd45a promotes DNA demethylation through TDG. *Nucleic Acids Res.* **43**, 3986-3997 (2015).

37. R. J. Hayward, J. W. Marsh, M. S. Humphrys, W. M. Huston, G. S. A. Myers, Chromatin accessibility dynamics of Chlamydia-infected epithelial cells. *Epigenetics & Chromatin* **13**, 45 (2020).

38. E. Schutyser, S. Struyf, J. Van Damme, The CC chemokine CCL20 and its receptor CCR6. *Cytokine Growth Factor Rev.* **14**, 409-426 (2003).

39. E. Homsak, D. Gruson, Soluble ST2: A complex and diverse role in several diseases. *Clin. Chim. Acta* **507**, 75-87 (2020).

40. R. Adami, D. Bottai, S-adenosylmethionine tRNA modification: unexpected/unsuspected implications of former/new players. *International Journal of Biological Sciences* **16**, 3018-3027 (2020).

41. M. Ohmer *et al.*, Infection of HeLa cells with Chlamydia trachomatis inhibits protein synthesis and causes multiple changes to host cell pathways. *Cell Microbiol* **21**, e12993 (2019).

42. H. Agaisse, I. Derré, A C. trachomatis Cloning Vector and the Generation of C. trachomatis Strains Expressing Fluorescent Proteins under the Control of a C. trachomatis Promoter. *PLoS ONE* **8**, e57090 (2013).

43. M. A. Scidmore, Cultivation and laboratory maintenance of *Chlamydia trachomatis*. *Curr Protocols Microbiol* 10.1002/9780471729259.mc11a01s00, 11A11.11-11A11.25 (2005).

44. J. Schindelin *et al.*, Fiji: an open-source platform for biological-image analysis.

45. I. Arganda-Carreras *et al.*, Trainable Weka Segmentation: a machine learning tool for microscopy pixel classification.

46. D. Ershov *et al.*, TrackMate 7: integrating state-of-the-art segmentation algorithms into tracking pipelines.

47. A. Birmingham *et al.*, Statistical methods for analysis of high-throughput RNA interference screens. *Nature Methods* **6**, 569-575 (2009).

48. J. Rappsilber, M. Mann, Y. Ishihama, Protocol for micro-purification, enrichment, pre-fractionation and storage of peptides for proteomics using StageTips. *Nature Protocols* **2**, 1896-1906 (2007).

49. S. Tyanova, T. Temu, J. Cox, The MaxQuant computational platform for mass spectrometry-based shotgun proteomics. *Nat Protoc* **11**, 2301-2319 (2016).

50. Q. G. Gianetto, S. Wieczorek, Y. Couté, T. Burger, A peptide-level multiple imputation strategy accounting for the different natures of missing values in proteomics data. *bioRxiv* 10.1101/2020.05.29.122770, 2020.2005.2029.122770 (2020).

51. M. E. Ritchie *et al.*, limma powers differential expression analyses for RNA-sequencing and microarray studies. *Nucleic Acids Res* **43**, e47 (2015).

52. Q. Giai Gianetto *et al.*, Calibration plot for proteomics: A graphical tool to visually check the assumptions underlying FDR control in quantitative experiments. *PROTEOMICS* **16**, 29-32 (2016).

53. Q. Giai Gianetto, "Statistical Analysis of Post-Translational Modifications Quantified by Label-Free Proteomics Across Multiple Biological Conditions with R: Illustration from SARS-CoV-2 Infected Cells" in Statistical Analysis of Proteomic Data: Methods and Tools, T. Burger, Ed. (Springer US, New York, NY, 2023), 10.1007/978-1-0716-1967-4_12, pp. 267-302.

54. S. Perrin, C. Firmo, S. Lemoine, S. Le Crom, L. Jourdren, Aozan: an automated post-sequencing data-processing pipeline. *Bioinformatics* **33**, 2212-2213 (2017).

55. C. The Galaxy, The Galaxy platform for accessible, reproducible and collaborative biomedical analyses: 2022 update. *Nucleic Acids Res.* **50**, W345-W351 (2022).

56. A. M. Bolger, M. Lohse, B. Usadel, Trimmomatic: a flexible trimmer for Illumina sequence data. *Bioinformatics* **30**, 2114-2120 (2014).

57. B. Langmead, C. Wilks, V. Antonescu, R. Charles, Scaling read aligners to hundreds of threads on general-purpose processors. *Bioinformatics* **35**, 421-432 (2019).

58. J. Feng, T. Liu, B. Qin, Y. Zhang, X. S. Liu, Identifying ChIP-seq enrichment using MACS. *Nature Protocols* **7**, 1728-1740 (2012).

59. C. S. Ross-Innes *et al.*, Differential oestrogen receptor binding is associated with clinical outcome in breast cancer. *Nature* **481**, 389-393 (2012).

60. G. Yu, L.-G. Wang, Q.-Y. He, ChIPseeker: an R/Bioconductor package for ChIP peak annotation, comparison and visualization. *Bioinformatics* **31**, 2382-2383 (2015).

61. A. R. Quinlan, I. M. Hall, BEDTools: a flexible suite of utilities for comparing genomic features. *Bioinformatics* **26**, 841-842 (2010).

62. I. Dunham *et al.*, An integrated encyclopedia of DNA elements in the human genome. *Nature* **489**, 57-74 (2012).

63. J. Ernst, M. Kellis, ChromHMM: automating chromatin-state discovery and characterization. *Nature Methods* **9**, 215-216 (2012).

64. G. Yu, L.-G. Wang, Y. Han, Q.-Y. He, clusterProfiler: an R Package for Comparing Biological Themes Among Gene Clusters. *OMICS: A Journal of Integrative Biology* **16**, 284-287 (2012).

65. T. D. Schmittgen, K. J. Livak, Analyzing real-time PCR data by the comparative CT method. *Nature Protocols* **3**, 1101-1108 (2008).

66. A. G. Torres, O. Reina, C. Stephan-Otto Attolini, L. Ribas de Pouplana, Differential expression of human tRNA genes drives the abundance of tRNA-derived fragments. *Proceedings of the National Academy of Sciences* **116**, 8451-8456 (2019).

67. R Core Team (2019) R: A Language and Environment for Statistical Computing. (R Foundation for Statistical Computing, Vienna, Austria).

LEGENDS TO THE FIGURES

Fig. 1. ***C. trachomatis* infection induces protein hypermethylation late in infection**. **A**. Cells were infected at MOI=1 with *C. trachomatis* serovar L2 for 48 h before fixation, permeabilization and staining with the indicated antibodies. DAPI staining of DNA allows for the detection of host nuclei and bacteria. *Chlamydia* inclusions are circled for reference. Bar, 10 μm **B**. Intensities for the indicated marks were quantified in the nuclei of non-infected and infected samples. The p-value of a Welch's t-test is shown ****: P < 0.0001 **C**. Fluorescence intensity measurements were normalized using Z-normalization. r= Pearson's coefficient of correlation **D**. Mouse derived organoids infected for 40 h with GFP-expressing *C. trachomatis* serovar L2 (top) or for 30 h with GFP-expressing *C. muridarum* (bottom) were fixed and stained for H3K9me3 (purple). Arrow heads point to nuclei with increased H3K9me intensity. Quantification of the intensity of the signal in nuclei of infected cells and of neighboring non infected cells is shown. The p-value of a Welch's t-test is shown. Bars, 50 μm. **E**. Volcano-plot of the relative enrichment of methylated host proteins in cells infected with *C. trachomatis*. The site of methylation (on R or K) is indicated for the proteins that are significantly hypomethylated (green quadrant) or hypermethylated (orange quadrant) in infected cells. Proteins or methylated peptides that were recovered in only one condition are absent from this representation (Table S1).

Fig. 2. **Histone hypermethylation correlates with bacterial proliferation**. **A**. HeLa cells were infected with *C. trachomatis* serovar L2 (MOI=1) for the indicated time before fixation, permeabilization and staining for H3K4me3 and H4K20me3. DAPI staining of DNA allows for the detection of infected cells, the inclusions are labeled with an asterisk. Bar, 10 μm. **B**. HeLa cells were infected with *C. trachomatis* L2 expressing GFP at MOI=0.2 and treated with the indicated concentration of doxycycline 24 hpi. Infectious forming units (IFUs) collected 48 hpi were quantified by reinfecting fresh HeLa cells as described in the methods. **C**. HeLa cells were infected with *C. trachomatis* serovar L2 at MOI=2 before fixation, permeabilization and staining as in **A**. Positive nuclei were defined as nuclei with fluorescence intensity greater than 2-fold the mean intensity of nuclei of non-infected samples. **D**. HeLa cells were infected with *C. trachomatis* L2 expressing mCherry for 48 h before fixation, permeabilization and staining for H3K9me3. An automated pipeline was used to discriminate infected and non-infected cells (See Methods). The mean fluorescence intensity of mCherry per inclusion is shown for infected cells with a low level of H3K9me3 signal (signal < 2-fold mean H3K9me3 signal in nuclei of non-infected cells) and with a high level of H3K9me3 signal (signal > 2-fold mean H3K9me3 signal in nuclei of non-infected cells). The p-value of a Welch's t-test is shown ****: P < 0.0001.

Fig. 3. **The activities of histone demethylases are sub-optimal in late *C. trachomatis* infected cells A**. Cells were infected with *C. trachomatis* serovar L2 for 48 h before isolation of the nuclei. SAM concentrations were normalized to protein content. Each dot represents an independent experiment. The p-value of a ratio paired t-test is indicated. **B**. Cells were infected with mCherry (blue) expressing *C. trachomatis* serovar L2. After 24 the culture medium was refreshed with or without 2 μM JIB-04. Cells were fixed 48 hpi, permeabilized and stained for H4K20me3 (green). DNA was labeled with DAPI (white). Bar, 50 μm. **C**. (*left*) H4K20me3 mean fluorescence intensity in nuclei of non-infected or infected cells treated 24 hpi with the indicated concentration of JIB-04 and fixed and stained 48 hpi as in A. Black bars indicate the mean. The p-value of Welsch's t-test are shown. (*right*) Positive nuclei were defined as nuclei with H4K20me3 intensity greater than two times the mean intensity of nuclei of non-infected cells from the same culture condition. The percentage of positive nuclei in each sample and the p-value of proportion comparison tests are shown ****, P < 0.0001; ***, P < 0.001; **, P < 0.01; *, P < 0.05; n.s., not significant. **D**. Cells were infected with mCherry (blue) expressing *C.*

trachomatis serovar L2. After 24 h the culture medium was left untouched (control) or refreshed with the addition of 5 mM DMKG, solvent alone (DMSO) or 100 μM ferric ammonium citrate (iron). Cells were fixed 48 hpi, permeabilized and stained for H3K4me3 (green) and H4K20me3 (red). DNA was stained with DAPI (display in white). Bar, 50 μm. **E**. The dot plots show the intensities for the indicated mark in nuclei of infected and non-infected cells. The p-value of Welch's t-tests are shown. The histograms display the percentages of positive nuclei, scored as in **C**. The p-value of proportion comparison tests are shown. **F**. Cells were transfected with HA-tagged KDM4A or Tsg5' as negative control and infected 3 h later with mCherry (displayed in blue) expressing *C. trachomatis* L2. Cells were fixed 48 h later, permeabilized and stained for HA and for the indicated histone methylation mark. DNA was stained with DAPI (white). Merged images are displayed, bar is 50 μm. The dot plots display the indicated relative mean methylation intensities of nuclei from infected cells. The histograms display the percentages of positive nuclei in the transfected infected cells. Cells were considered transfected when the HA signal in the nucleus was greater than the two-fold value of the mean intensity in nuclei in non-transfected cells of duplicate wells. Nuclei were scored positive as in C. The p-value of proportion comparison tests are shown.

Fig. 4. **H3K4me3 and H3K9me3 chromatin landscape**. **A.** Profile of the H3K4me3 ChIP-seq signal (read density) from merged biological replicates, i.e pileups of the H3K4me3 enrichment relative to chromatin input (subtraction mode, input from IP of bam files) in non-infected (NI) and infected HeLa cells on genomic loci defined as 3kb upstream and downstream of annotated Transcriptional Start Site (TSS) of genes (NCBI RefSeq). **B**. Boxplots showing reads coverage (log2(CPM+1), CPM counts per million, bin=500 bp) from H3K4me3, H3K9me3 ChIP-seq experiments and input in non-infected (NI) and infected HeLa cells. The median and the p-value (Wicoxon test) is indicated within each boxplot. Outliers are not shown for clarity.

Fig. 5 **DMKG supplementation modifies the global transcriptional responses to infection**. **A**. Transcripts from infected and non-infected samples, supplemented or not with 5 mM DMKG 24 hpi, and extracted 48 hpi were analyzed by microarray. Two by two comparisons of differentially expressed genes are shown (cut-off: 2-fold difference). **B**. Venn diagram showing about one third of the differentially regulated genes upon infection were no longer differentially regulated with DMKG supplementation. **C**. (*Left*) Microarray result: histograms display relative mRNA levels for 5 DGEs compared to uninfected cells. (*Middle*) Validation by RT-qPCR: Samples were prepared in the same conditions as the microarray samples. Specific set of primers for the indicated genes were used to measure transcripts levels by RT-qPCR normalized to actin transcripts following the ΔΔCt method. Each experiment was performed repeated at least four times. The data are presented as relative mRNA levels compared to uninfected cells and shown as the mean ± SD. Statistical comparisons were obtained using contrast analysis after linear modeling, 2 by 2 multiple-testing and P-value adjustment (See methods for details). ****, $P < 0.0001$; ***, $P < 0.001$; **, $P < 0.01$. (*Right*) Same except that cells were treated with 1 μM JIB-04. **D**. Cells were infected with *C. trachomatis* L2 for 48 hpi, with or without treatment with 1 μM JIB-04 24 hpi. Levels of $tRNA^{Gly\text{-}GCC}$ and $tRNA^{Arg\text{-}UCG}$ measured by Northern blot are expressed relative to 5S RNA and U6 snRNA. See the method section for statistical analysis of the data.

Fig. 6. **JIB-04 modulates the innate response to infection *in vivo***. **A**. Schematic view of animal infections. JIB-04 treatment was administered intra-peritoneally (i.p.) and infections with *C. muridarum* were intravaginal. **B**. Bacterial load was measured on DNA extracted from vaginal lavages at D3 and in the lower genital tracts at D6 and normalized to host DNA. Unpaired t-test showed no

statistical difference. **C**. Vaginal lavages were used to measure transcripts levels for the indicated genes by RT-qPCR, normalized to *actin* following the $\Delta\Delta$Ct method. Data are expressed relative to samples from non-infected non treated animals (NI). Statistical comparisons were obtained using contrast analysis after linear modeling, 2 by 2 multiple-testing and P-value adjustment (See methods for details). **D**. Same as in **C**, RNA being extracted from lower genital tracts excised at D6.

Table S1. Relative abundance of host methylated proteins 48 hpi with *C. trachomatis*.

Table S2. Relative abundance of host proteins 48 hpi with *C. trachomatis*.

Table S3. ChIP analyses.

Table S4. Differentially expressed host genes 48 hpi with *C. trachomatis*.

Table S5. DMKG sensitive genes in *C. trachomatis* infection.

Table S6. Antibodies used.

Table S7. Oligonucleotides used.

Table S8. CTL2M340rs59 variants, identified by genotyping.

Figure 1

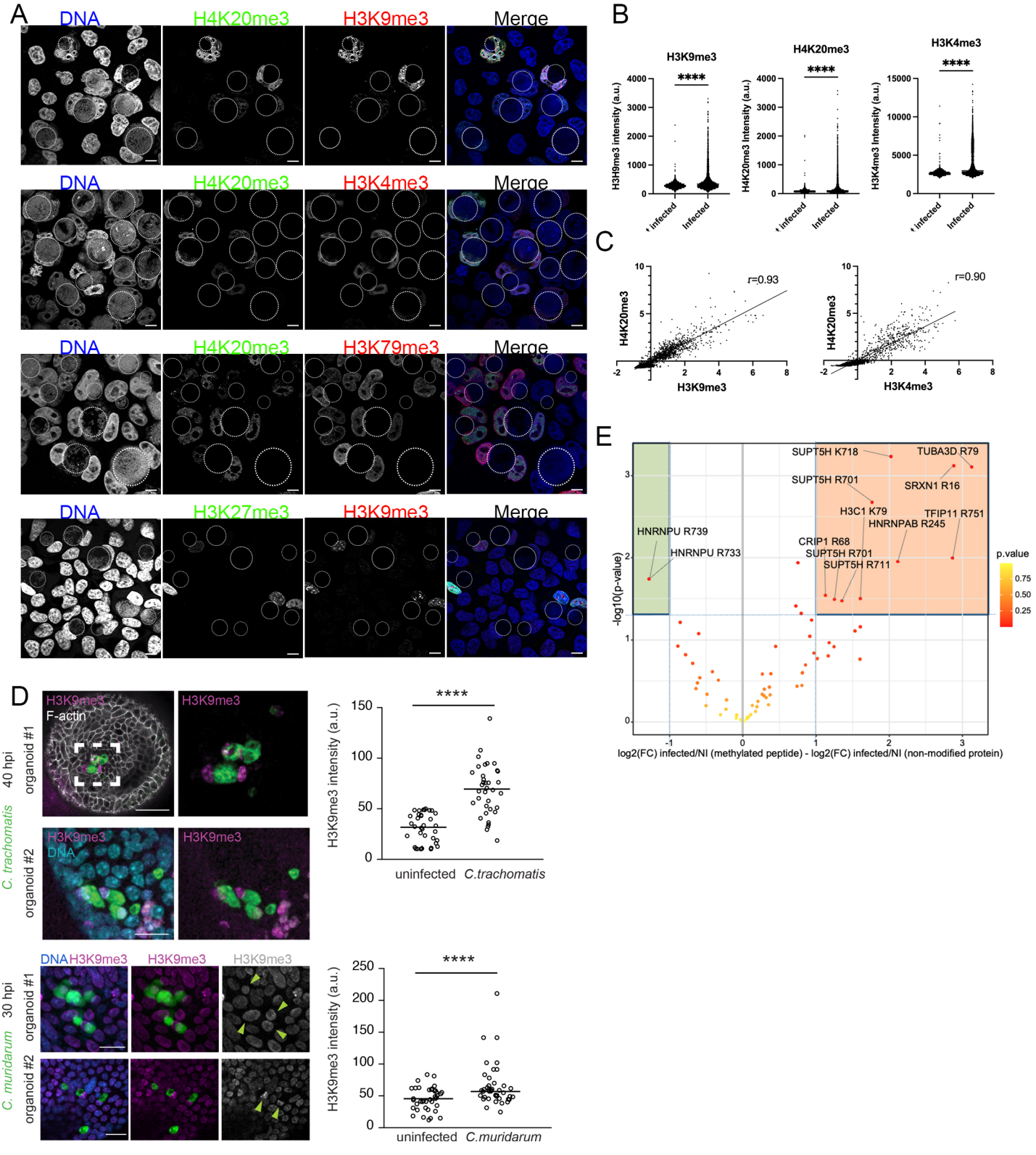
A
DNA
H4K20me3
H3K9me3
Merge
DNA
H4K20me3
H3K4me3
Merge
DNA
H4K20me3
H3K79me3
Merge
DNA
H3K27me3
H3K9me3
Merge
B
H3K9me3
H4K20me3
H3K4me3
****
H3H9me3 intensity (a.u.)
H4K20me3 Intensity (a.u.)
H3K4me3 Intensity (a.u.)
Infected
C
r=0.93
r=0.90
H4K20me3
H3K9me3
H3K4me3
E
SUPT5H K718
TUBA3D R79
SUPT5H R701
SRXN1 R16
H3C1 K79
TFIP11 R751
HNRNPAB R245
HNRNPU R739
HNRNPU R733
CRIP1 R68
SUPT5H R701
SUPT5H R711
p.value
-log10(p-value)
log2(FC) infected/NI (methylated peptide) - log2(FC) infected/NI (non-modified protein)
D
H3K9me3
F-actin
DNA
40 hpi
organoid #1
organoid #2
C. trachomatis
H3K9me3 intensity (a.u.)
uninfected
C.trachomatis
30 hpi
C. muridarum
C.muridarum

Figure 2

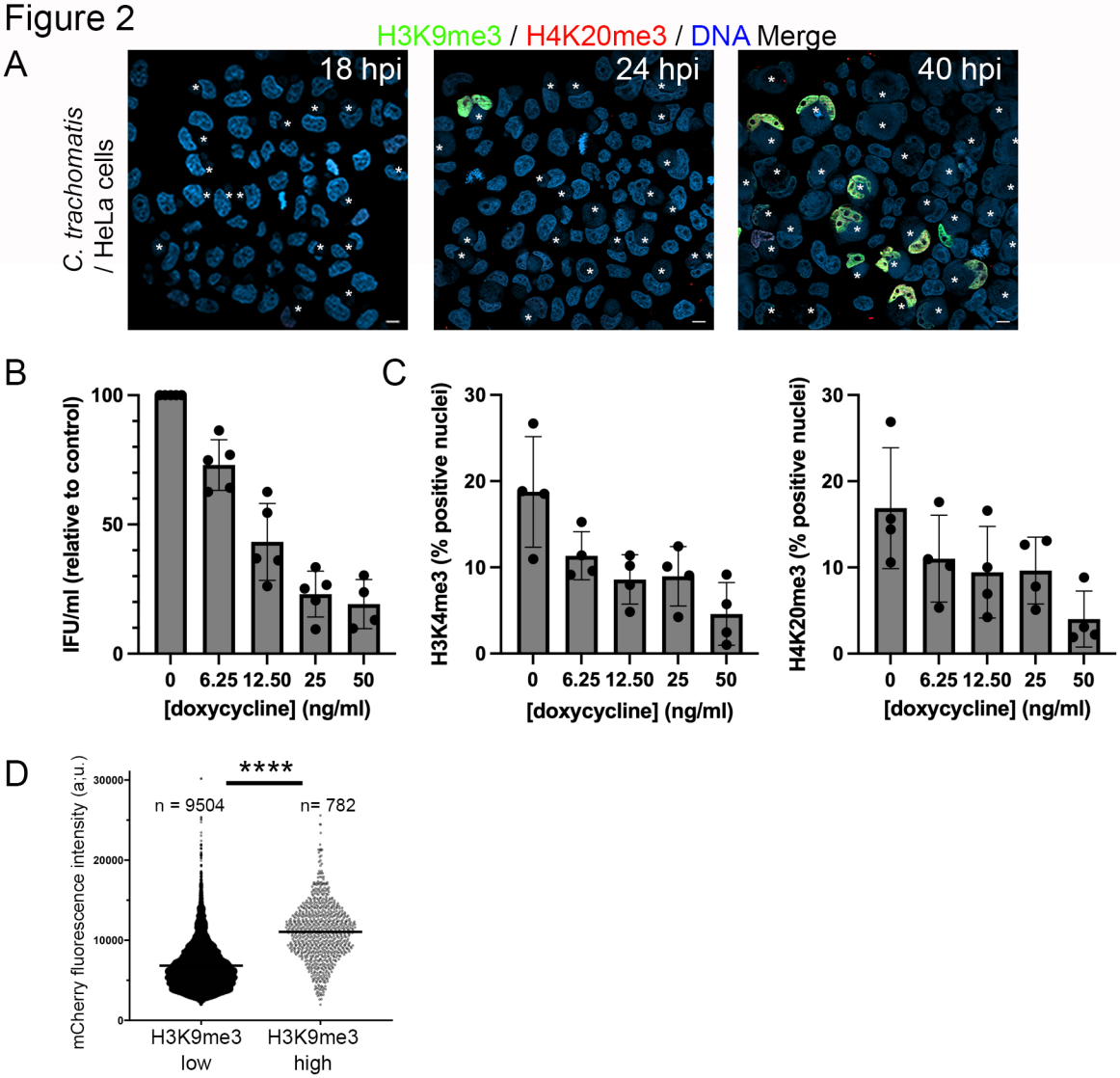
A
H3K9me3 / H4K20me3 / DNA Merge
18 hpi
24 hpi
40 hpi
C. trachomatis / HeLa cells
B
IFU/ml (relative to control)
100
50
0
0
6.25
12.50
25
50
[doxycycline] (ng/ml)
C
H3K4me3 (% positive nuclei)
30
20
10
0
0
6.25
12.50
25
50
[doxycycline] (ng/ml)
H4K20me3 (% positive nuclei)
30
20
10
0
0
6.25
12.50
25
50
[doxycycline] (ng/ml)
D
mCherry fluorescence intensity (a.u.)
30000
20000
10000
0
****
n = 9504
n= 782
H3K9me3 low
H3K9me3 high

Figure 3

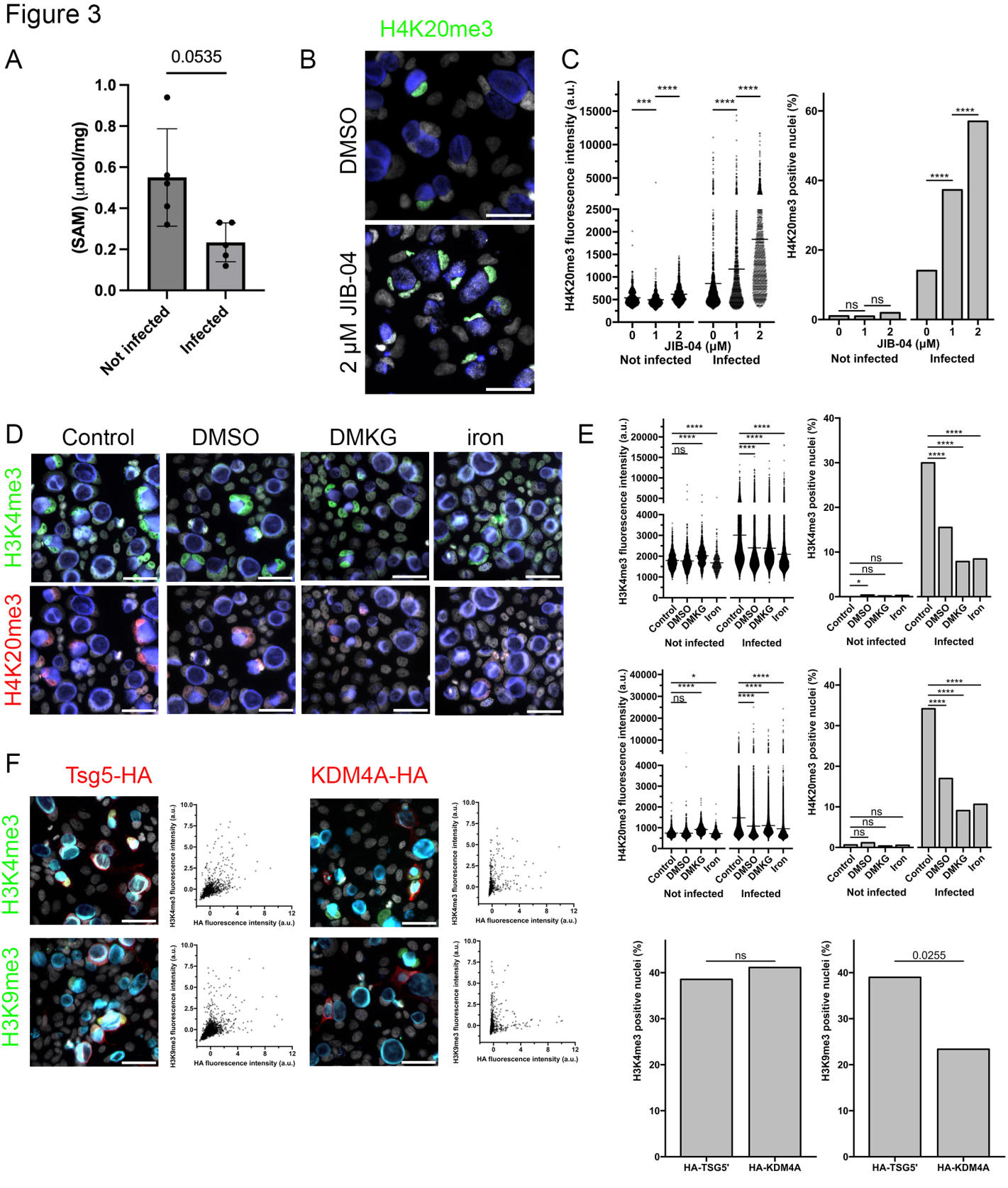
A
0.0535
(SAM) (µmol/mg)
Not infected
Infected
B
H4K20me3
DMSO
2 µM JIB-04
C
H4K20me3 fluorescence intensity (a.u.)
JIB-04 (µM)
Not infected
Infected
H4K20me3 positive nuclei (%)
D
Control
DMSO
DMKG
iron
H3K4me3
H4K20me3
E
H3K4me3 fluorescence intensity (a.u.)
H3K4me3 positive nuclei (%)
H4K20me3 fluorescence intensity (a.u.)
H4K20me3 positive nuclei (%)
F
Tsg5-HA
KDM4A-HA
H3K4me3
H3K9me3
HA fluorescence intensity (a.u.)
H3K4me3 positive nuclei (%)
H3K9me3 positive nuclei (%)
ns
0.0255
HA-TSG5'
HA-KDM4A

Figure 4

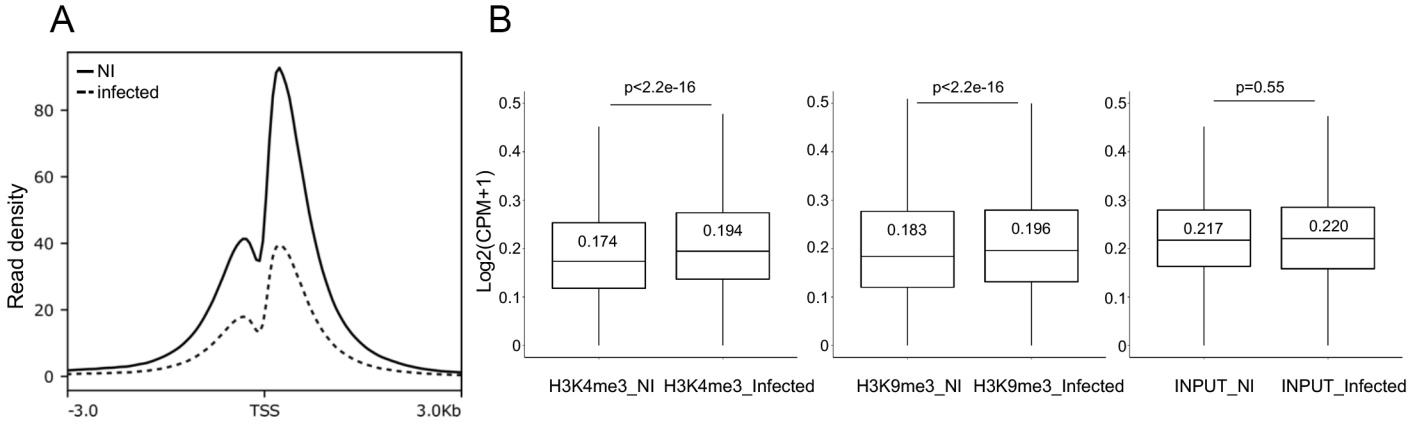
A
NI
infected
Read density
80
60
40
20
0
-3.0
TSS
3.0Kb
B
Log2(CPM+1)
p<2.2e-16
0.174
0.194
H3K4me3_NI
H3K4me3_Infected
p<2.2e-16
0.183
0.196
H3K9me3_NI
H3K9me3_Infected
p=0.55
0.217
0.220
INPUT_NI
INPUT_Infected
0.5
0.4
0.3
0.2
0.1
0

Figure 5

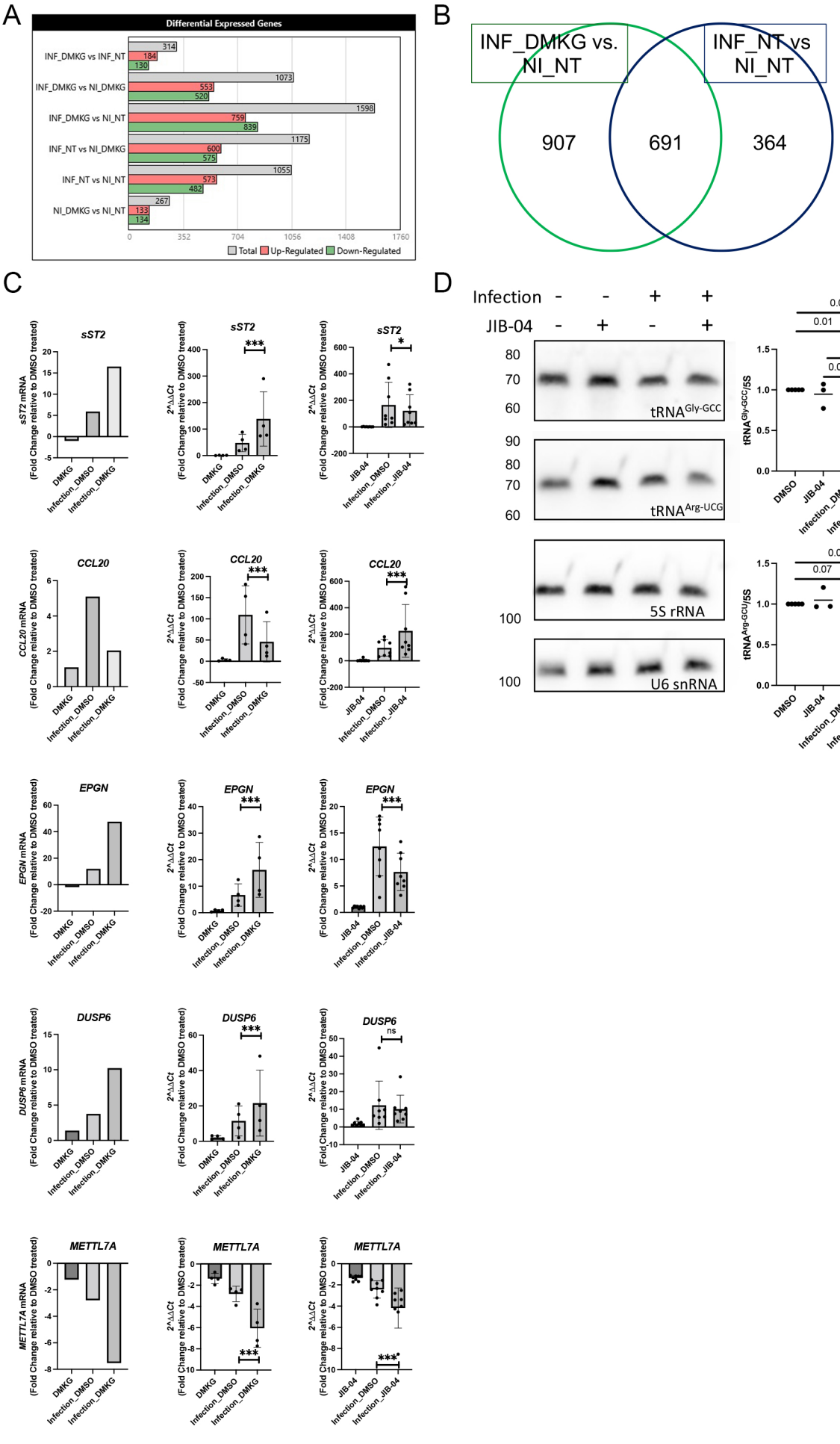
A
Differential Expressed Genes
INF_DMKG vs INF_NT
INF_DMKG vs NI_DMKG
INF_DMKG vs NI_NT
INF_NT vs NI_DMKG
INF_NT vs NI_NT
NI_DMKG vs NI_NT
314
184
130
1073
553
520
1598
759
839
1175
600
575
1055
573
482
267
133
134
0
352
704
1056
1408
1760
Total
Up-Regulated
Down-Regulated
B
INF_DMKG vs. NI_NT
INF_NT vs NI_NT
907
691
364
C
sST2
CCL20
EPGN
DUSP6
METTL7A
sST2 mRNA (Fold Change relative to DMSO treated)
2^ΔΔCt (Fold Change relative to DMSO treated)
DMKG
Infection_DMSO
Infection_DMKG
JIB-04
Infection_JIB-04
***
*
ns
D
Infection
JIB-04
tRNA Gly-GCC
tRNA Arg-UCG
5S rRNA
U6 snRNA
tRNA Gly-GCC/5S
tRNA Gly-GCC/U6
tRNA Arg-GCU/5S
tRNA Arg-GCU/U6
DMSO
JIB-04
Infection_DMSO
Infection_JIB-04
0.01
0.05
0.03
0.07

Figure 6

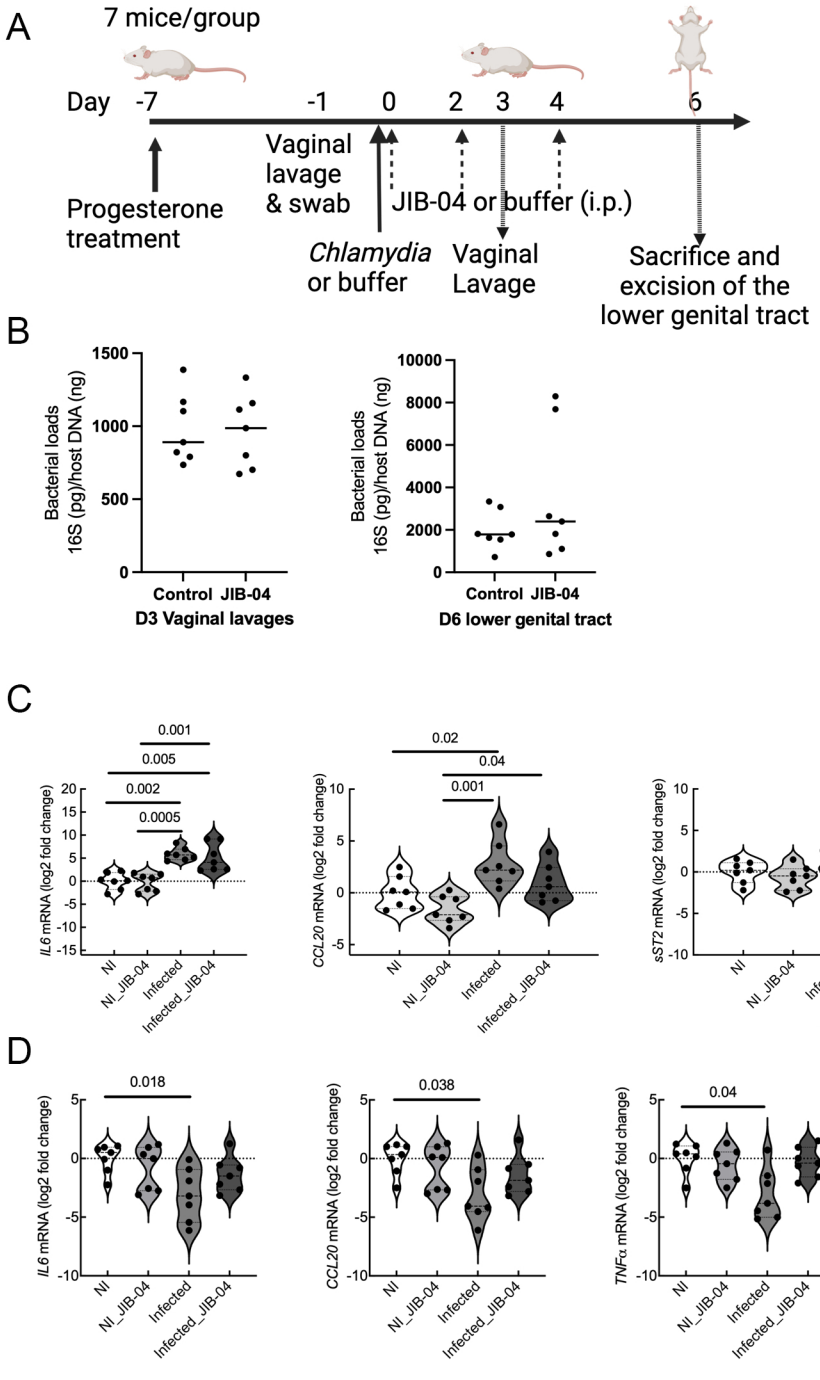
A
7 mice/group
Day -7 -1 0 2 3 4 6
Progesterone treatment
Vaginal lavage & swab
JIB-04 or buffer (i.p.)
Chlamydia or buffer
Vaginal Lavage
Sacrifice and excision of the lower genital tract
B
Bacterial loads 16S (pg)/host DNA (ng)
Control JIB-04
D3 Vaginal lavages
D6 lower genital tract
C
IL6 mRNA (log2 fold change)
CCL20 mRNA (log2 fold change)
sST2 mRNA (log2 fold change)
NI
NI_JIB-04
Infected
Infected_JIB-04
D
IL6 mRNA (log2 fold change)
CCL20 mRNA (log2 fold change)
TNFα mRNA (log2 fold change)
IL1β mRNA (log2 fold change)

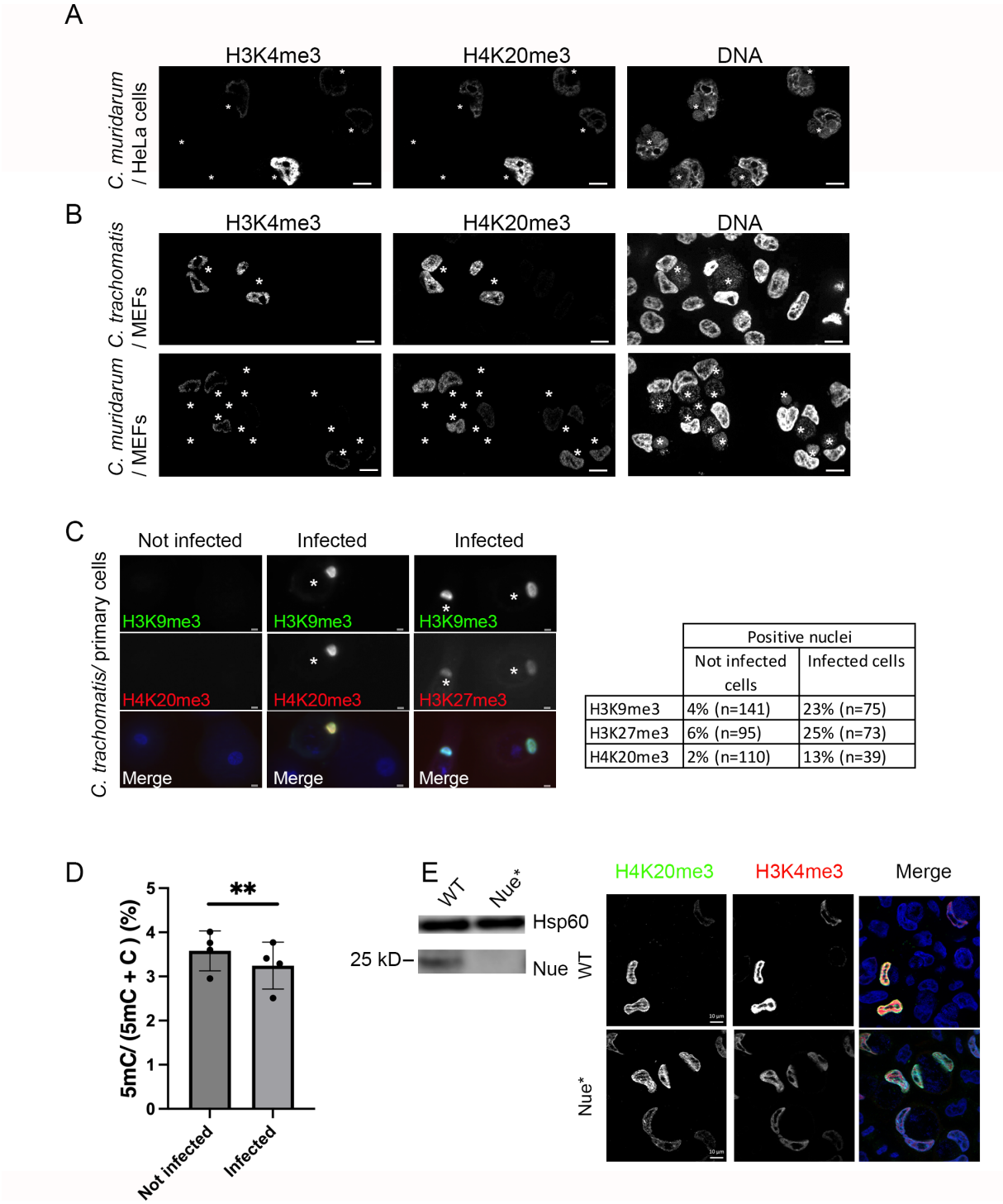

	Positive nuclei	
	Not infected cells	Infected cells
H3K9me3	4% (n=141)	23% (n=75)
H3K27me3	6% (n=95)	25% (n=73)
H4K20me3	2% (n=110)	13% (n=39)

Fig. S1. **Histone hypermethylation occurs in various cell type and is independent of Nue**. **A**. HeLa cells were infected with *C. muridarum* for 48 h before fixation, permeabilization and staining for H3K4me3 and H4K20me3. DNA was stained with DAPI, inclusions are highlighted with an asterisk. **B**. MEFs were infected with *C. trachomatis* L2 (top) or *C. muridarum* (bottom) for 48 h before proceeding as in A. **C**. Primary human epithelial cells isolated from the ectocervix were infected for 48 h with *C. trachomatis* serovar L2 before proceeding as in **A**. Right panel shows quantification of relative distribution of histone marks. **D**. Nuclei were isolated from cells infected for 48 h with *C. trachomatis* L2 or from control cells prior to measurement of DNA methylation by mass spectrometry. Results of four independent experiments are shown, with mean ± SD, and the P-value of the Student's paired t-test is indicated (**P < 0.01). **E**. Cells were infected for 48 h with *C. trachomatis* L2 WT or with a mutant that does not express Nue (Nue*=CTL2M340rs59, see methods), fixed, permeabilized and stained with the indicated antibodies. Absence of NUE expression in cell lysates 24 hpi was verified by western blot (left). Antibodies against the chlamydial protein Hsp60 were used to control for infection levels.

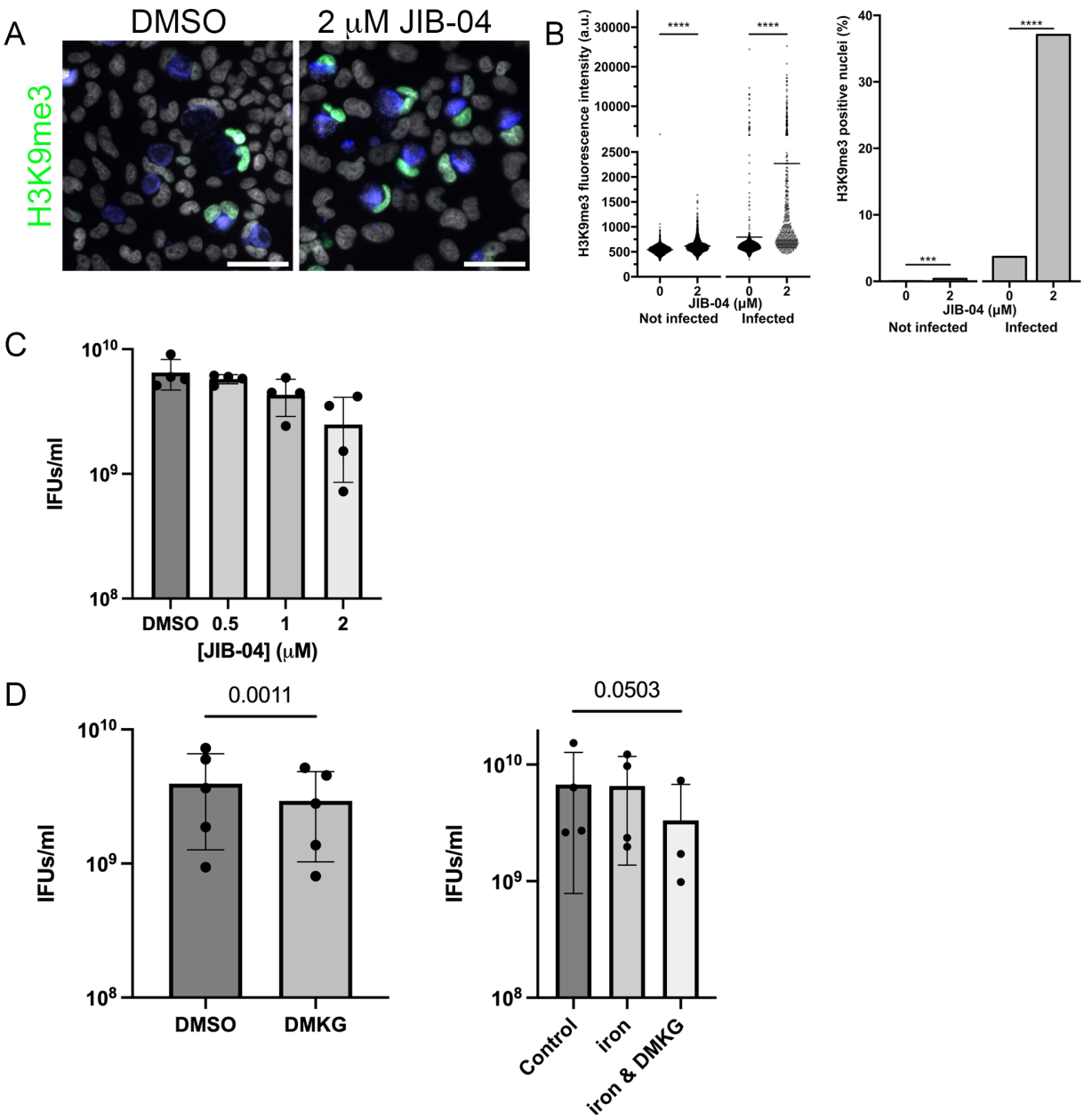

Fig. S2. **Effect of JIB-04, DMKG or iron on histone methylation and on infection**. **A**. Cells were infected with mCherry expressing *C. trachomatis* serovar L2 (blue). Twenty-for hours later the culture medium was renewed with or without 2 μM JIB-04. Cells were fixed 48 hpi, permeabilized and stained for H3K9me3 (green). DNA was labeled with DAPI (grey). Bar, 50 μm. **B** H3K9me3 mean fluorescence intensity in nuclei of non-infected or infected cells treated 24 hpi with the indicated concentration of JIB-04 and fixed and stained 48 hpi. Black bars indicate the mean. The percentage of positive nuclei in each sample and the p-value of Welsch's t-test are shown ****, $P < 0.0001$; ***, $P < 0.001$. **C**. HeLa cells were infected with *C. trachomatis* L2 expressing GFP at MOI=0.2 and treated with the indicated concentration of JIB-04 24 hpi. Infectious forming units (IFUs) collected 48 hpi were quantified by reinfecting fresh HeLa cells as described in the methods. **D**. HeLa cells were infected with *C. trachomatis* L2 expressing GFP at MOI=0.2. At 24 hpi the culture medium was replaced with medium supplemented with 5 mM DMKG (or DMSO alone), 100 μM ferric ammonium citrate, or a combination of both. Infectious forming units were measured 48 hpi. P-values of ratio-paired t-tests are shown when < 0.05.

A

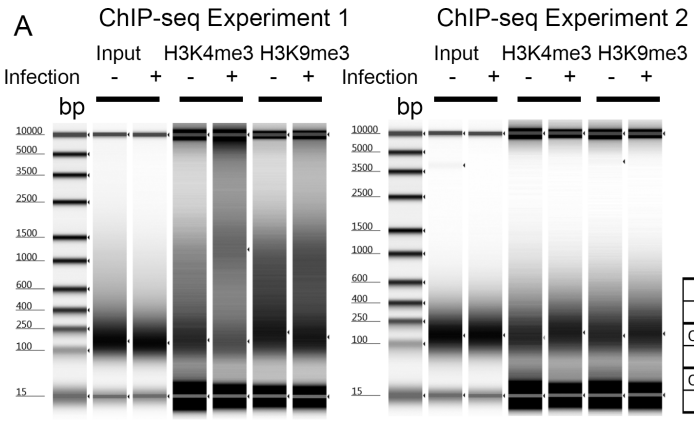

	Infection	Experiment 1	Experiment 2
		Concentration (pg/µl)	
Input	-	3970	2300
	+	2950	2640
ChIP_H3K4me3	-	292	171
	+	525	278
ChIP_H3K9me3	-	863	198
	+	933	252

B

		Experiment 1		Experiment 2	
		Reads	Currated Peaks	Reads	Currated Peaks
ChIP_H3K4me3	-	89,642,372	18,420	112,750,886	38,446
	+	88,518,854	22,002	131,873,696	32,109
ChIP_H3K9me3	-	77,460,690	53,318	117,650,964	103,853
	+	116,528,378	62,937	119,949,837	83,225

C

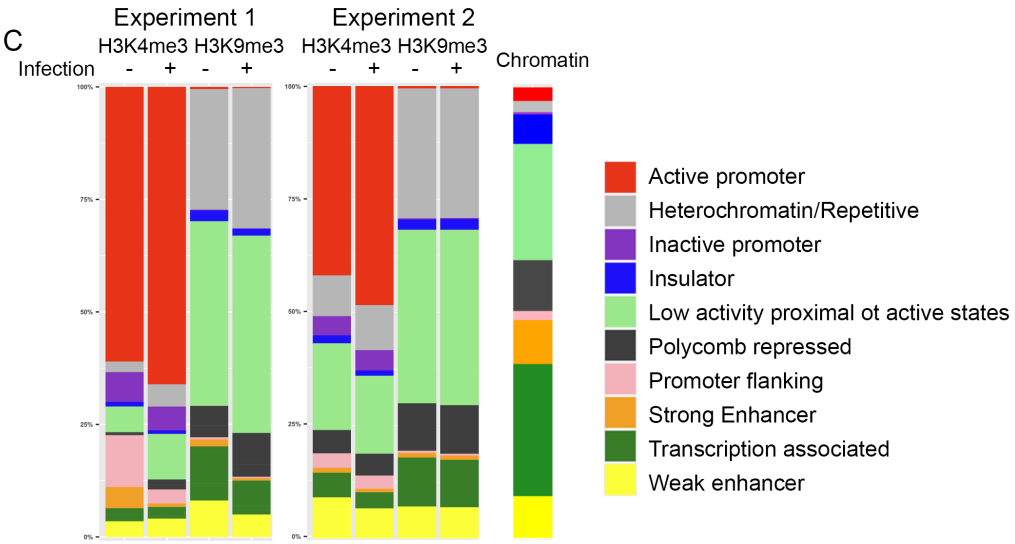

D

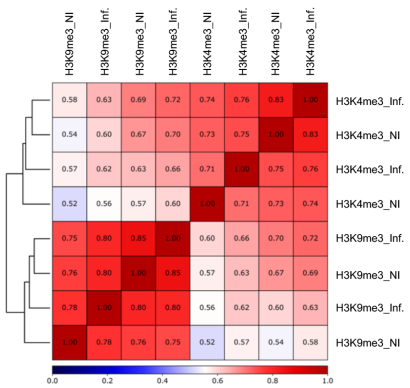

Fig. S3. **Quality controls for the ChIP experiments. A**. Electophoresis profile of input DNA isolated from infected and uninfected cells and corresponding ChIP with antibodies to the indicated histone marks. The DNA concentrations measured in each lane are reported in the table. **B**. Number of reads and peaks analyzed for each experiment. **C**. Distribution of genomic sites enriched in H3K4me3 and H3K9me3 marks. The functional annotation was based on the chromatin states established from ChromHMM (ChromHMM track from ENCODE/Broad Institute). The relative abundance in HeLa cells of each chromatin state is shown on the right. **D**. Hierarchically clustering of correlation matrix of H3K4me3 and H3K9me3 ChIP-seq replicates (1 and 2) performed in non-infected (NI) and infected (Infected) HeLa cells. Spearman correlations were calculated in deepTools (the multiBamSummary (Galaxy Version 3.5.4+galaxy0) was followed with plotCorrelation (Galaxy Version 3.5.4+galaxy0) using the read counts split into 500-bp bins across the human genome.

Table S6. Antibodies used

	Target	Species	Supplier	Catalog #
Primary Antibodies	H3K9me3	Rabbit	Abcam	ab8898
	H4K20me3	Mouse	Abcam	ab78517
	H3K27me3	Mouse	Bp biosciences	25243
	H3K4me3	Rabbit	Diagenode	C15410003
	H3K79me2	Rabbit	Abcam	ab3594
	HA	Rat	Roche Diagnostics	Clone 3F10 #1 867 423
	Nue	Rabbit	Subtil lab	Pennni et al 2010
	Hsp60	Rabbit	Subtil lab	
Secondary Antibodies	Alexa Fluor TM 488 goat anti-rabbit IgG (H+L)	Goat	Invitrogen	A-11034
	Alexa Fluor TM 647 goat anti-rabbit IgG (H+L)	Goat	Invitrogen	A-21244
	Alexa Fluor TM 488 goat anti-mouse IgG (H+L)	Goat	Invitrogen	A-11029
	Alexa Fluor TM 647 goat anti-mouse IgG (H+L)	Goat	Invitrogen	A-21235
	Alexa Fluor TM 488 goat anti-rat IgG (H+L)	Goat	Invitrogen	A-11006

Table S7. Oligonucleotides

Oligonucleotides for RT-qPCR (infection in human cells)

Gene	Sequence
sST2	GGCACACCGTAAGACTAAGTAG
	CAATTTAAGCAGCAGAGAAGCTCC
CCL20	CTGGCTGCTTTGATGTCAGT
	CGTGTGAAGCCCACAATAAA
EPGN	TTTGGGAGTTCCAATATCAGTCTA
	TGTGATTGGAGGTGTTACAGTCA
METTL7A	CTGCAGTTTGAGCGCTTTGT
	GGATCCAGGACTTGTTGCCA
DUSP6	TCACTGTGACTGTGGCTTACCTTATG
	GCAGCTGACCCATGAAGTTGAAGT
Actin	GGACTTCGAGCAAGAGATGG
	GCAGTGATCTCCTTCTGCATC

Oligonucleotides for Northern blots

tRNA-Gly-GCC	GGCAGGCGAGAATTCTACCACTGAA
tRNA-Arg-UCG	GCGGCAGGACTCGAACCTG
5S rRNA	CCGACCCTGCTTAGCTTCC
U6 snRNA	TTGCGTGTCATCCTTGCGCAGG

Oligonucleotides for RT-qPCR (infection in mice)

Gene	Sequence
16S (*Chlamydia*)	TGGATGAGGCATGCAAGTC
	TACTAACCCTTCCGCCACTAAA
mActin	AGCTGTGCTATGTTGCTCTAGACTT
	CACTTCATGATGGAATTGAATGTAG
mIL6	TAGTCCTTCCTACCCCAATTTCC
	TTGGTCCTTAGCCACTCCTTC
mCCL20	TTTTGGGATGGAATTGGACAC
	TGCAGGTGAAGCCTTCAACC
msST2	GCATGATAAGGCACACCATAA
	ACACAGAGAGGGGAAGGATA
mTNFα	TAGCCAGGAGGGAGAACAG
	CCACAAGCAGGAATGAGAAG
mIL1β	ATGGCAACTGTTCCTGAACTCAA
	CAGGACAGGTATAGATTCTTTCC

Table S8. CTL2M340rs59 variants, identified by genotyping

Genome position	Locus tag L2/434/Bu	Locus tag D/UW-3/CX	Gene name L2/434/Bu	Gene product L2/434/Bu	SNV type	Amino acid substitution	Reference base	Variant base
31647	CTL0024	CT655	*kdsA*	2-dehydro-3-deoxyphosphooctonate aldolase	SYNONYMOUS		G	A
45497	CTL0038	CT669	*cdsN*	Flagellar type ATPase (probable beta subunit)	SYNONYMOUS		G	A
129156	CTL0105	CT736		Conserved hyporthetical protein	Non-neutral	G94R	G	A
129786	CTL0106	CT737	*nue*	SET domain containing protein	NONSENSE	W71*	C	T
412397	CTL0331	CT075	*dnaN*	DNA polymerase III, beta chain	SYNONYMOUS		G	A
583383	CTL0489	CT237	*fabG*	3-oxoacyl-[acyl-carrier protein] reductase	SYNONYMOUS		C	T
727008	CTL0610	CT356		Conserved hypothetical protein	Neutral	E200K	C	T
763628	CTL0646	CT390	*dapL*	DAP (diaminopimelic acid) aminotransferase	Neutral	R186H	G	A
777726	CTL0657	CT400	*sucB*	Lipoamide acyltransferase component (E2) of branched-chain alpha-keto acid dehydrogenase complex	SYNONYMOUS		C	T
813780	CTL0684	CT425		Conserved hypothetical protein	Neutral	G432S	G	A
856581	CTL0721	CT461		Putative metallo-phosphoesterase	Neutral	S292F	C	T
886766	CTL0753	CT492	*coaE*	Dephospho-CoA kinase	Neutral	D154N	C	T
907368	CTL0774	CT512	*rpsE*	SSU ribosomal protein S5P	SYNONYMOUS		C	T
947484					NON-CODING		G	A
975723	CTL0846	CT583	*gp6D*	Virulence plasmid protein pGP6-D-related protein	SYNONYMOUS		C	T
1014167	CTL0879	CT615	*rpoD*	RNA polymerase sigma factor	Neutral	D50N	C	T